CHAPTER 9

THE INTERPRETATION OF EPR PARAMETERS

9.1 INTRODUCTION

An adequate interpretation of the parameters of the spin hamiltonian usually requires the application of molecular quantum mechanics. We already noted the explicit expressions for matrices **g** and **D** (Eqs. 4.41 and 4.42), as well as the relation of the isotropic and anisotropic parts of the hyperfine matrix to $|\psi(0)|^2$ (Eq. 2.38) and $\langle r^{-3} \rangle$ (Eq. 5.6*a*). In general, for quantitative interpretation, a large-scale analysis by computer is required. Happily, however, relatively simple and successful analytical quantum-mechanical models exist that serve well for tutorial purposes. This chapter introduces some of these techniques. One key aspect for EPR analysis is to understand which, among the infinite number of electronic states, is the ground state, and to realize its properties. Part of the power of EPR spectroscopy is that (unlike optical spectroscopy) it deals only with spin transitions within a single electronic state.

Before going further, we need to tighten up our knowledge of spin densities and unpaired-electron populations.[1] Like other densities, spin densities ρ_s can be evaluated in selected local regions and thus depend on location within a paramagnetic atom or molecule. Thus they can be integrated over part or the total volume, yielding dimensionless physically useful parameters ρ called the 'unpaired-electron populations' on the species considered.

There can be a simple proportionality between spin density $\langle \rho_s \rangle_n$ at a nucleus n and unpaired-electron population ρ (see Section 5.6). For example,

Electron Paramagnetic Resonance, *Second Edition*, by John A. Weil and James R. Bolton
Copyright © 2007 John Wiley & Sons, Inc.

$\langle \rho_s \rangle_p = \rho |\psi|_p^2$ for atomic hydrogen; both functions are evaluated at the proton p [1,2]. In general, however, both are multi-electron functions.

Consider, as an example, a Gd(3+) ion ($S = \frac{7}{2}$) embedded in some complex. The spin density is very high at the cation, with only small magnitudes occurring on the nearest-neighbor ligands. The unpaired-electron population here is 7. In most free radicals, $\rho = 1$. More examples follow.

In situations where the anisotropic hyperfine splitting on some nucleus n can be considered to be purely dipolar and is uniaxial (see Eqs. 5.48 and 5.49 near the limit $f = 1$), the distance r between the electron-spin species, requiring unpaired-electron population correction factors $k(e)$, and external nucleus n carrying a point magnetic population [no corrections; $k(n) = 1$ for all our purposes] can be approximated by

$$r = \left(\frac{\mu_0}{4\pi}\right) \frac{g\beta_e g_n \beta_n k(e) k(n)}{T_\perp} \tag{9.1}$$

and thus this distance can be estimated [3]. Matrix $\mathbf{T}$ is defined in Eq. 5.8, and is expressed in energy units. We note that $T_\perp$ varies as approximately r^{-3} and may contain geometry factors. The distance r is, of course, set by the electromagnetic quantum-mechanical interactions between all atoms present, and is hardly affected by the magnetic dipole-dipole effect. The above Equation 9.1 may be compared to its isotropic equivalent, Eq. 2.51.

Since we have considered the transition ions in Chapter 8, we focus in this chapter on the interpretation of EPR parameters from free radicals and triplet states. Free radicals are classified into organic radicals, inorganic radicals and point defects in crystalline solids. A short discussion of EPR in metals and semiconductors is also included.

It is useful to distinguish between σ-type and π-type free radicals. The former type features one unpaired electron in an orbital having no nodal plane, whereas the latter has one unpaired electron in a molecular orbital that has such a symmetry element. Often the nodal plane in π-type radicals extends over several atoms; this arises from overlap between the p orbitals on each atom and implies that the unpaired electron is delocalized over the system. By contrast, σ-type radicals tend to have unpaired electrons primarily localized on one atom.

9.2 π-TYPE ORGANIC RADICALS

Among the various molecular-orbital theoretical approaches [4], Hückel molecular-orbital (HMO) theory is the simplest. We shall apply this theory to some relatively simple paramagnetic species, with a view to understanding the isotropic hyperfine splittings exhibited by these π-type radicals. Some details of HMO theory are to be found in Appendix 9A at the end of this chapter.

Most of the radicals examined in Chapter 3 are conjugated molecules, containing paired electrons in low-lying σ orbitals and the remainder in π orbitals. The distinguishing characteristic in modeling such compounds, diamagnetic or

paramagnetic, is the overlap of p orbitals on adjacent atoms. Such overlapping permits the electrons in these orbitals to be delocalized as a π system over the molecular skeleton. One may, to a good approximation, describe the energy states of these electrons separately from those of the others, in terms of molecular orbitals generated from linear combinations of the atomic $2p_z$ orbitals. For example, each of the six $2p_z$ orbitals in benzene has a node in the molecular plane, defined to be the xy plane. Hence the molecular orbitals arising from combinations of $2p_z$ orbitals (Tables 9A.1 and 9A.2) are referred to as *π orbitals*. The ground state of benzene consists of three π orbitals containing six electrons, with the other three π orbitals unoccupied.

Each unpaired electron of a π-type radical is expected to be distributed over the molecular framework. For example, in the benzene monoanion the average relative probability of finding its unpaired electron in the vicinity of any one carbon atom is $\frac{1}{6}$, as required by symmetry. For other monocyclic radicals a similar uniform distribution should be found. The equivalence of each position in a given monocyclic radical leads to the ^{1}H hyperfine splitting patterns shown in Figs. 3.3*a–h*.

For radicals with lower symmetry, there is no such obvious guide to the unpaired-electron distribution. The HMO approach provides valuable guidance toward determining this distribution. The information of interest is contained in the expression for the particular spatial molecular orbital

$$\psi_i = \sum_{j=1}^{n} c_{ij}\phi_j \tag{9.2}$$

occupied by the unpaired electron. Here n is the number of atomic orbitals ϕ_j, which are orthonormal. Since ψ_i is normalized, one has

$$\sum_{j=1}^{n} |c_{ij}|^2 = 1 \tag{9.3}$$

The magnitude squared of the coefficient c_{ij} is the relative probability that the electron in molecular orbital ψ_i is in atomic orbital ϕ_j. Thus $|c_{ij}|^2$ measures the unitless unpaired π-electron population ρ_j 'on' atom j when this atom bears only a single orbital occurring in ψ_i:

$$\rho_j = |c_{ij}|^2 \tag{9.4}$$

It follows that

$$\sum_{j=1}^{n} \rho_j = 1 \tag{9.5}$$

As an example, consider the radical anion of 1,3-butadiene [5]. The EPR spectrum displayed in Fig. 3.7*a* was analyzed on the basis of a quintet of lines of relative intensities $1:4:6:4:1$ with a proton hyperfine splitting of 0.762 mT;

each line of the quintet is split further into a 1 : 2 : 1 triplet with a proton hyperfine splitting of 0.279 mT. The considerable difference between the two splitting 'constants' suggests a highly non-uniform unpaired-electron distribution.

The butadiene anion has five π electrons. Reference to the molecular orbitals of Table 9A.1 shows that, consistent with the Pauli exclusion principle, the unpaired electron must reside in ψ_3. From Eq. 9.4 the unpaired-electron populations are found to be $\rho_1 = \rho_4 = 0.36$ and $\rho_2 = \rho_3 = 0.14$. Thus HMO theory predicts that the end carbon atoms should have the higher unpaired-electron densities. We note that these are indeed the positions at which the larger proton hyperfine splittings are observed and that the ratio of the hyperfine splittings, $a_1/a_2 = 2.7$,[2] agrees satisfactorily with the ratio of the unpaired-electron populations, $\rho_1/\rho_2 = 2.6$.

This correspondence seems to point to some sort of linear relation between the (isotropic) proton hyperfine splitting parameters a_k and the unpaired π-electron populations of the carbon atoms in π-type organic radicals. Indeed, such a relation has been proposed [6–9]; it may be written for proton k as

$$a_k = Q\rho_k \tag{9.6}$$

where ρ_k is the unpaired π-electron population at the adjacent carbon atom k and Q is a proportionality constant expressed in magnetic-field units. The origin of Eq. 9.6 is considered in Section 9.2.4. An examination of Fig. 9.1 shows that for most π-type

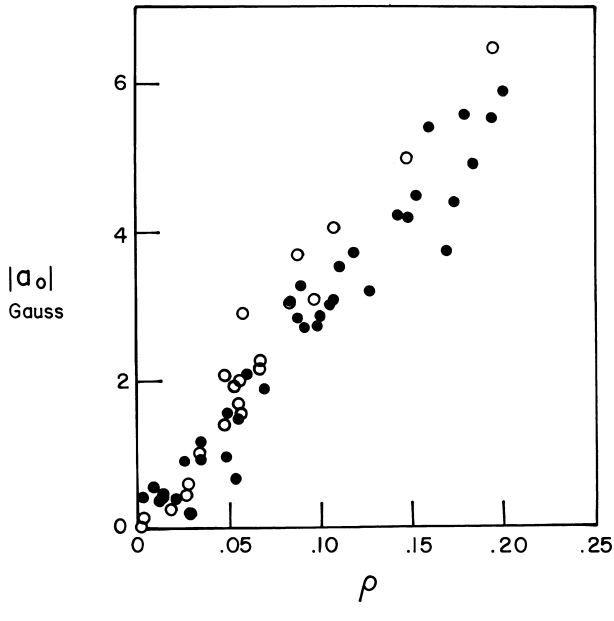

FIGURE 9.1 Experimental proton hyperfine splitting parameters $|a_0|$ versus HMO unpaired-electron populations ρ for a group of aromatic hydrocarbon radical ions. Open circles refer to positive ions and filled circles to negative ions. [After I. C. Lewis, L. S. Singer, *J. Chem. Phys.*, **43**, 2712 (1965).]

organic radicals the correlation (Eq. 9.6) is good. A similar and even more extensive data set, featuring a good linear plot of the hydrogen 1*s*-orbital unpaired-electron population against the adjacent carbon $2p_z$-orbital unpaired-electron population, has been presented by Pople et al. [2]. Here, rather than the crude HMO method, the much more advanced INDO molecular-orbital technique was utilized.[3]

Theoretical estimates of Q place it in the range from -2 to -3 mT. The significance of the negative sign is explained in Section 9.2.4. The first confirmation of the negative sign of Q in Eq. 9.6 was obtained by an analysis of the splittings in the malonic acid radical (HOOC—CH—COOH), created by irradiation of the acid [10]. The simplest π radical is, of course, methyl (CH_3). It has $S = \frac{1}{2}$ and exhibits a proton hyperfine splitting constant of -2.304 mT [11]. This agrees nicely with Eq. 9.6 with $\rho = 1$, providing strong evidence that CH_3 indeed is planar (cf. CF_3, Section 9.3).

In certain other molecules, it is possible to establish a value of Q semi-empirically from the experimental hyperfine splittings. For instance, in the cyclic polyene radicals C_5H_5 (cyclopentadienyl) (**I**), $C_6H_6^+$, C_7H_7 (cycloheptatrienyl) (**II**) and $C_8H_8^-$, which are planar, the unpaired-electron population is known from the molecular symmetry. Thus an experimental determination of the hyperfine splitting constant a in these molecules provides an estimate of Q. Table 9.1 gives the experimental values of a and the corresponding values of Q for these monocyclic radicals.

(**I**) cyclopentadienyl radical

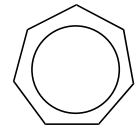

(**II**) cycloheptatrienyl radical

There is an appreciable variation in Q for these monocyclic radicals. If one compares the values for the two neutral radicals or for the two negatively charged

TABLE 9.1 Proton Hyperfine Splitting Parameters for Monocyclic Radicals

Radical	Temperature[a] (K)	a^H (mT)	Q (mT)	Reference
C_5H_5	~200	0.600	3.00	*b*
$C_6H_6^+$	298	0.428	2.57	*c*
$C_6H_6^-$	173	0.375	2.25	*d*
C_7H_7	298	0.395	2.77	*e*,*f*
$C_8H_8^-$	~298	0.321	2.57	*g*

[a] Some of the hyperfine splittings have been found to be temperature-dependent.[b,c,f]

[b] R. W. Fessenden, S. Ogawa, *J. Am. Chem. Soc.*, **86**, 3591 (1964). See also: M. Iwasaki, K. Toriyama, K. Nunome, *J. Chem. Soc., Chem. Commun.*, 320 (1983).

[c] M. K. Carter, G. Vincow, *J. Chem. Phys.*, **47**, 292 (1967).

[d] J. R. Bolton, *Mol. Phys.*, **6**, 219 (1963).

[e] A. Carrington, I. C. P. Smith, *Mol. Phys.*, **7**, 99 (1963).

[f] G. Vincow, M. L. Morrell, W. V. Volland, H. J. Dauben Jr., F. R. Hunter, *J. Am. Chem. Soc.*, **87**, 3527 (1965).

[g] T. J. Katz, H. L. Strauss, *J. Chem. Phys.*, **32**, 1873 (1960).

radicals, the variation is much smaller, correctly suggesting that the charge on the radical has some effect on Q.

An understanding of the hyperfine properties of protons in conjugated hydrocarbon radicals is aided by classifying these as alternant or non-alternant. A molecule (and its ions) is defined as alternant if one may label alternate positions of the carbon skeleton with an asterisk and have no two adjacent positions both 'starred' or both 'unstarred'. All linear systems are alternant, as are also those cyclic systems that have no rings made up of an odd number of atoms, for example, anthracene (Fig. 3.9). In contrast, the C_5H_5 and C_7H_7 radicals are non-alternant, as is the azulene anion (**III**). When there is more than one way of starring atoms, by convention one adopts that designation that gives the largest number of starred atoms. If the numbers of starred and of unstarred positions are equal, the hydrocarbon is called *even-alternant*; if not, it is called *odd-alternant*.

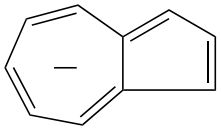

(**III**) azulene anion

Odd-alternant hydrocarbon radicals have a very useful property that permits rapid calculation of the unpaired-electron populations without actually determining molecular-orbital coefficients. As an example, consider the non-bonding semi-occupied orbital ψ_4 of the benzyl radical ($C_6H_5CH_2$) (**IV**)

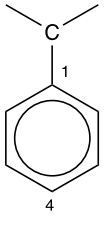

(**IV**) benzyl radical

$$\psi_4 = 0\phi_1 - 0.378\phi_2 + 0\phi_3 + 0.378\phi_4 + 0\phi_5 - 0.378\phi_6 + 0.756\phi_7 \qquad (9.7)$$

Having starred this odd-alternant radical appropriately, one assigns equal and opposite coefficients about unstarred positions having two neighbors. One begins by assigning the coefficient $-c$ to atom 2, $+c$ to 4, $-c$ to 6, and finally $+2c$ to 7 to cancel the contributions from atoms 2 and 6. The squares of the coefficients must sum to unity; hence $c = 1/\sqrt{7} = 0.378$. The unpaired-electron population is then $\frac{1}{7}$ at atoms 2, 4 and 6, and $\frac{4}{7}$ at atom 7. The simple procedure employed here for determining ρ values saves much effort, as compared with the direct HMO calculation (Problem 9A.4). This procedure may also be applied to even-alternant hydrocarbons if non-bonding orbitals are present (e.g., cyclooctatetraene).

TABLE 9.2 Benzyl Radical[a] Hyperfine Parameters a_i (in mT)

Protons on Carbon Atoms	^{1}H Splitting Parameters a_i	
	Experimental[b,c]	HMO Calculated
2,6	−0.49	−0.40
4	−0.61	−0.40
7 (CH_3)	−1.59	(−1.59)
3,5	+0.15	0

[a] See structure **IV**.
[b] W. T. Dixon, R. O. C. Norman, *J. Chem. Soc.*, 4857 (1964).
[c] A. Carrington, I. C. P. Smith, *Mol. Phys.*, **9**, 137 (1965).

The experimental hyperfine splittings for the benzyl radical (**IV**) are given in Table 9.2. Using the splitting for position 7 to fix Q, the hyperfine splittings for positions 2, 4 and 6 are calculated to be −0.40 mT. No hyperfine splitting would be expected for protons at positions 3 and 5 because the atomic orbital coefficients are zero. The significance of the small positive hyperfine splitting observed for protons at these positions is discussed later in this chapter. Although there are significant deviations from predictions, one can regard the calculated values as being in remarkable agreement with experiment, considering the crudity of the approach.

9.2.1 Anions and Cations of Benzene and Some of Its Derivatives

Benzene represents a classic hydrocarbon for study of the effects of substituents in removing the degeneracies of energy levels and for modifying the unpaired-electron distribution in its ±1 ions. In common with numerous other monocyclic systems, the π HMO molecular orbital of lowest energy in benzene is non-degenerate; the next four higher orbitals form degenerate pairs (Table 9A.2). It is customary to use the group-theoretic labeling (group D_{6h}). Here it is sufficient to note that e always refers to degenerate pairs of orbitals, whereas a and b refer to non-degenerate orbitals. The set of six molecular orbitals for benzene is given in Table 9A.2 in order of *increasing* energy (bottom to top). The bracketed orbitals are degenerate. Note that in the a orbital there is no change of sign and hence no vertical nodal plane. This is the orbital of lowest energy. In increasing order of energy, the e_1 orbitals have two oppositely signed (+/−) regions and a nodal plane, the e_2 orbitals two nodal planes, whereas the b orbital, that of highest energy, has three nodal planes.

In the benzene anion, the extra (7th) π electron is in the e_2 set of orbitals, whereas in the cation an electron is missing from the e_1 set. Hyperfine splitting data for the anion allow us to show how occupancy of the e_2 orbitals changes with substitution of the benzene ring.

The liquid-solution EPR spectrum of the benzene anion at −100°C is shown in Fig. 3.4. The spectrum consists of seven lines with intensities characteristic of hyperfine interaction from six equivalent protons. This result is expected from the symmetry of the molecule, but it is instructive to see how it arises from the Hückel

molecular orbitals given in Table 9A.2. The six π electrons of the neutral benzene go into the three bonding molecular orbitals, but the addition of an extra electron to make the benzene anion creates a new problem. The lowest unoccupied molecular orbital in benzene is doubly degenerate. Hence the unpaired electron is expected to occupy equally the two e_2 antibonding molecular orbitals.[4] The coefficients at each of the atoms for these orbitals are given at the right of Fig. 9.2. It is evident that the wavefunction of one e_2 state, A, is antisymmetric with respect to reflection in a vertical plane passing through carbon atoms labeled 1 and 4; S, the other, is symmetric with respect to reflection in the same plane. A is termed the 'antisymmetric' orbital and S the 'symmetric' orbital.

The total unpaired-electron population at a given position is obtained by taking one-half the sum of the electron populations (squares of coefficients) at that position for each of the two orbitals. For example, at positions 1 and 2, $\rho_1 = \frac{1}{2}\left(0 + \frac{1}{3}\right) = \frac{1}{6}$ and $\rho_2 = \frac{1}{2}\left(\frac{1}{4} + \frac{1}{12}\right) = \frac{1}{6}$. Thus all positions are equivalent.

Although in the benzene anion the orbitals A and S are, in the first approximation, equally occupied, the population balance is extremely delicate. The introduction of substituents serves to remove the degeneracy, that is, makes one orbital more energetic than the other. Thus the effect of substituents on the EPR spectrum of the benzene anion is best understood by considering the limiting spectra anticipated when the unpaired-electron distribution approximates that of the A or of the S orbitals.

The EPR spectrum in Fig. 9.2 is that of the *p*-xylene anion [12]. It is significant that the splitting from the CH_3 protons is too small to be resolved. This phenomenon is to be expected when the unpaired electron resides predominantly in the A orbital.

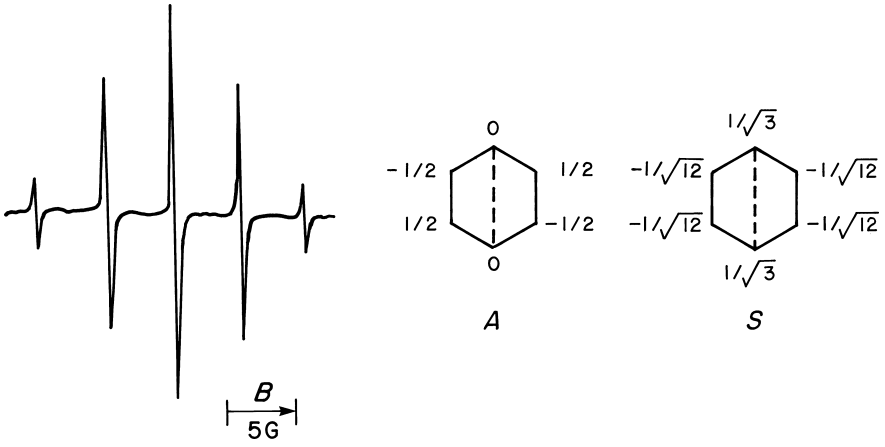

FIGURE 9.2 EPR spectrum of the *p*-xylene anion, with the atomic orbital coefficients of the antisymmetric (A) and symmetric (S) molecular orbitals of benzene at the right. The symmetry is defined with respect to the perpendicular plane (dashed) passing through the center of the molecule. Solvent is dimethoxyethane, and temperature is $-70°$C. [After J. R. Bolton, A. Carrington, *Mol. Phys.*, **4**, 497 (1961).]

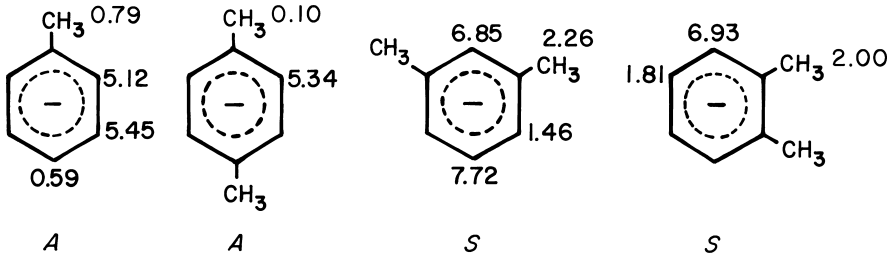

FIGURE 9.3 Proton hyperfine splittings a (in gauss) for various methyl-substituted benzene anions. Symbols A and S indicate whether the antisymmetric or the symmetric π orbitals lie lowest for these molecules. [After J. R. Bolton, A. Carrington, *Mol. Phys.*, **4**, 497 (1961); J. R. Bolton, *J. Chem. Phys.*, **41**, 2455 (1964).]

The hyperfine splittings that have been observed for various methyl-substituted benzenes are given in Fig. 9.3. The data show that the introduction into benzene of even one CH_3 group removes the degeneracy of A and S. The methyl groups are rapidly rotating, that is, effectively linear. The electronic properties of the substituent determine whether the A or the S orbital has the lower energy. The methyl group is considered to be electron-releasing in conjugated systems. For the toluene anion, the A orbital has a vertical nodal plane through the 1 and 4 positions, whereas the S orbital has a large unpaired-electron population $\left(\frac{1}{3}\right)$ at these positions. Repulsion between the electrons on the methyl group and the large negative charge at positions 1, 2, 5 and 6 in the S orbital causes the latter to be destabilized relative to A.

The Q value of -2.25 mT for the benzene anion may be used to estimate the toluene anion hyperfine splittings. Because of the node through the 1 and 4 positions, one should expect little or no hyperfine splitting from the methyl protons or the proton *para* to the methyl group. An unpaired-electron population of $\frac{1}{4}$ should give rise to a hyperfine splitting of $\sim$0.56 mT. The measured hyperfine splittings (Fig. 9.3) show that the unpaired-electron distribution does approximate that of the A orbital.

Even the substitution of a deuterium nucleus for a proton in the benzene anion is sufficient to bring about a measurable split of the energies of the S and A orbitals as indicated by small departures of the proton hyperfine splittings from those in the benzene anion [13].

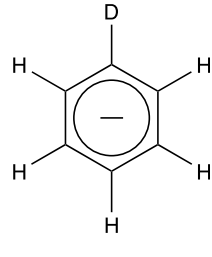

(**V**) benzene-d_1 anion

9.2.2 Anions and Cations of Polyacenes

For some of the EPR spectra analyzed in Chapter 3, it was not possible to assign the observed hyperfine splittings on the basis of the spectrum alone. Thus, for the mono-anion of naphthalene (**VI**) (Fig. 3.8), it is not obvious which set of four equivalent protons should be assigned as yielding the larger hyperfine splitting. The same uncertainty is found for the two quintet splittings in the spectrum (Fig. 3.9) of the anion of anthracene (**VII**). It thus is very desirable to have a simple and rational basis for the assignment of these hyperfine splittings, as presented here. In addition, it is helpful that the relative magnitudes of hyperfine splittings can be predicted without making detailed calculations.

In the HMO approximation, alternant hydrocarbons have orbital energies symmetrically disposed about the central energy α. *Odd*-alternant hydrocarbons have a non-bonding orbital at this energy (e.g., Fig. 9A.1). Orbitals with energies symmetrically disposed about α involve the same atomic orbitals, with coefficients that have the same *absolute* magnitudes. Therefore the squares of the coefficients of the highest bonding orbital and of the lowest antibonding orbital of an even-alternant hydrocarbon are identical. Hence *the unpaired-electron distribution is predicted to be identical in the cation and anion radicals corresponding to a given diamagnetic parent*. This statement is often referred to as the *pairing theorem* and is found to apply to a high degree of approximation [14,15].

The EPR spectra of the anions and cations of some of the polyacenes [naphthalene (**VI**), anthracene (**VII**), tetracene (**VIII**) and pentacene (**IX**)] have been studied. The proton hyperfine splittings for these molecules are listed in Table 9.3. It is evident that the hyperfine splittings are similar for protons in corresponding positions in the anion and the cation of a given molecule. These results are in reasonable accord with the pairing theorem. The agreement in reality is even better than is apparent, since Q depends somewhat on the excess charge density [16,17].

9.2.3 *g* Factors of π Radicals

The g factors of π radicals have been the focus of considerable theoretical attention, basically using the theory outlined in Section 4.8. Typically, $g - g_e = (1 \text{ to } 4) \times 10^{-4}$. For aromatic radicals in the liquid phase, Stone [18,19] showed that

$$g - g_e = g_{(0)} + g_{(1)}\lambda + g_{(2)}\lambda^2 \tag{9.8}$$

where the $g_{(i)}$ are (semi-empirical) parameters and λ is the coefficient of the resonance integral β in the HMO of the unpaired electron. One can classify the excited states required (Eqs. 4.38 and 4.41) to calculate $\mathbf{g}$ into different types; for example, excitation of the odd π electron into an antibonding σ orbital, and excitation of any σ-bonding electron into the semi-occupied π orbital. The theory fits well except when there is a degenerate (or almost so) ground state, for example, for the benzene radical anion, in which case complex corrections (for vibronic coupling and ion pairing) must be made [20–22].

TABLE 9.3 Proton Hyperfine Splitting Parameters in Polyacene Anions and Cations

Molecule	Position	$\lvert a_+^{\mathrm{H}}\rvert$ (mT)	$\lvert a_-^{\mathrm{H}}\rvert$ (mT)
Naphthalene[a] (**VI**)	1	0.540	0.495
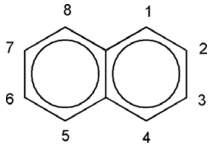	2	0.160	0.187
Anthracene[b] (**VII**)	9	0.6533	0.5337
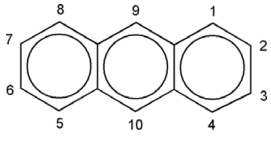	1	0.3061	0.2740
	2	0.1379	0.1509
Tetracene[c] (**VIII**)	5	0.5061	0.4226
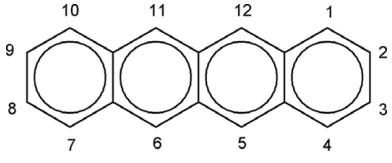	1	0.1694	0.1541
	2	0.1030	0.1162
Pentacene[d] (**IX**)	6	0.5083	0.4263
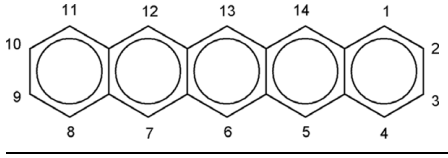	5	0.3554	0.3032
	1	0.0975	0.0915
	2	0.0757	0.0870

[a] (+) Estimated from simulating the X-band EPR spectrum taken in boric acid glass at ~300 K; G. Vincow, P. M. Johnson, *J. Chem. Phys.*, **39**, 1143 (1963) and G. S. Owen, G. Vincow, *J. Chem. Phys.*, **54**, 368 (1971); (−) N. M. Atherton, S. I. Weissman, *J. Am. Chem. Soc.*, **83**, 1330 (1961).

[b] (+) and (−) J. R. Bolton, G. K. Fraenkel, *J. Chem. Phys.*, **40**, 3307 (1964).

[c] (+) J. S. Hyde, H. W. Brown, *J. Chem. Phys.*, **37**, 368 (1962); (+) and (−) J. R. Bolton, unpublished work [see J. R. Bolton, *J. Chem. Phys.*, **71**, 3702 (1967)].

[d] (+) and (−) J. R. Bolton, *J. Chem. Phys.*, **46**, 408 (1967).

9.2.4 Origin of Proton Hyperfine Splittings

As discussed, it has been found for planar conjugated organic radicals that proton hyperfine splittings are proportional to the unpaired π-electron population on the carbon adjacent to the proton (Eq. 9.6). Isotropic proton hyperfine splittings were shown in Chapter 2 to arise when a net unpaired-electron density exists at the

proton. In π radicals, the unpaired electron can be considered to reside in a π-molecular orbital constructed from a linear combination of $2p_z$ carbon atomic orbitals. However, each such $2p_z$ orbital has a node in the plane of the molecule and, since this plane also contains the adjacent proton, there should be no unpaired-electron density at the proton and hence no hyperfine splitting. In spite of this node, the numerous spectra in Chapter 3 demonstrate that isotropic proton hyperfine splittings *do* occur in π radicals. Out-of-plane proton vibrations are found to give a negligible effect. Rather, the concept of unpaired-electron density must be reexamined in order to resolve this paradox. It was assumed that an electron in a conjugated molecule does not influence the other electrons in the radical. However, in reality the other electrons are affected. Thus, in some regions of the molecule, 'paired' electrons become slightly unpaired. (This is one of the several effects that go under the name of 'electron correlation'). Thus the actual *spin density* at the proton (Eq. 2.51) is not simply related to the nominal unpaired-electron population on the adjacent carbon atom. Factor Q in Eq. 9.6 brings in this effect, which we now discuss.

Consider a C—H fragment of a conjugated system. If spin α is assigned to the one electron in the $2p_z$ orbital on the carbon atom, there are two possibilities for assigning the spins in the C—H σ bond; these are shown in Fig. 9.4. Here it is assumed that the carbon atom has its $2p_z$ orbital perpendicular to the C—H bond; the $2p_x$ and $2p_y$ orbitals plus the $2s$ orbital of the carbon atom form trigonal sp^2 hybrids. The hydrogen atom bonds to one of these three coplanar hybrids.

If there were no electron in the $2p_z$ orbital, the electron configurations (*a*) and (*b*) of Fig. 9.4 would be equally probable; hence the spin density at the proton would be zero. However, when a $2p_z$ electron is present, say, with spin α, configurations (*a*) and (*b*) are no longer equally probable. This effect is often called *spin polarization*. It has been demonstrated from atomic spectroscopy that when two different, but equivalent, orbitals on the same atom are singly occupied by electrons, the more stable arrangement is the one with the electron spin components M_S equal (one of Hund's rules). Thus configuration (*a*), in which the two electrons shown on the

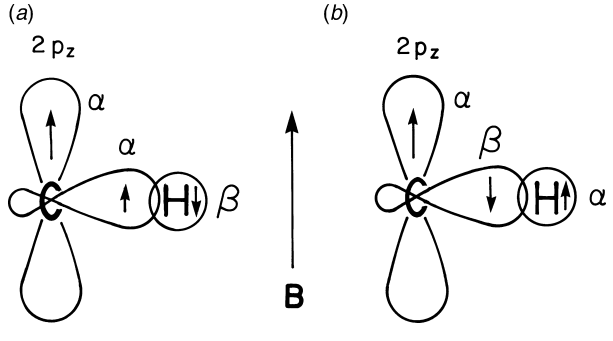

FIGURE 9.4 Possible electron-spin configurations in the σ-orbital bonding the carbon atom to the hydrogen atom in a C—H fragment, for a spin in the $2p_z$ orbital of that carbon: (*a*) spins parallel in the σ bonding orbital and the $2p_z$ orbital of carbon; (*b*) Corresponding spins antiparallel.

carbon atom have parallel spins, is more stable and hence more probable than (b), for which the spins are antiparallel; that is, as a consequence of the *positive* spin density at the carbon nucleus, there is a net *negative* electron-spin density (i.e., excess of β spin over α spin) at the proton. Conversely, if the spin state of the electron in the carbon p_z orbital is β, then a spin predominates at the proton. Detailed treatment of the effect demonstrates that Eq. 9.6 is close to quantitative [2,6–9], with Q negative. Of course, in a conjugated radical the unpaired-electron population ρ_i at a given carbon atom is less than unity. Note that for the ensemble of molecules, spin states β $\left(M_S = \frac{1}{2}\right)$ are the more populated (Fig. 1.2).

The concepts discussed above can be expressed elegantly and quantitatively in terms of a suitable mathematical formalism. We saw (Eq. 2.51) that the sign and magnitude of a_0 can be obtained quantum-mechanically by introduction of the spin-density operator $\hat{\rho}_s$. Here, for each nucleus,

$$\hat{\rho}_s(\mathbf{r}_s) = \langle \hat{S}_z \rangle^{-1} \sum_k \hat{S}_{kz}\, \delta(\mathbf{r}_k - \mathbf{r}_n) \tag{9.9}$$

is the spin-density operator, where the sum is over all electrons; $\hat{\mathbf{S}} = \sum_k \hat{\mathbf{S}}_k$ is the total electron-spin operator and $\langle \hat{S}_z \rangle$ is the expectation value $M_S = \sum_k M_{S_k}$ of $\sum_k \hat{S}_{kz}$ for the state $\psi(\mathbf{r}_k)$ considered (we assume $M_S \neq 0$). Clearly, ψ contains both spatial and electron-spin variables. The factor $\delta(\mathbf{r}_k - \mathbf{r}_n)$ is the famous Dirac delta 'function' (Section A.7) [4,23,24], here three-dimensional, with dimension of volume^{-1}. It has meaning only within a definite integral $\int_V F\, \delta\, dV$ of some spatial function $F(\mathbf{r}_k)$ (e.g., $\psi^* \psi$), which it sets to zero except at the single point $\mathbf{r}_k = \mathbf{r}_n$. Thus the integral becomes $F\big|_{\mathbf{r}_k = \mathbf{r}_n}$ when the volume V includes nucleus n.

9.2.5 Sign of the Proton Hyperfine Splitting Constant

The negative sign (Eq. 9.6) of Q implies that the hyperfine parameter a_k for the proton of a C—H fragment is negative, and that the spin density there is opposite in sign to that in the adjacent carbon $2p_z$ orbital.

Although this sign information can be obtained from comparison of the isotropic and anisotropic hyperfine couplings (Section 5.2 and Problem 5.11), another method, involving a verification of the signs by a proton magnetic resonance, is now examined.

This procedure involves the measurement of proton magnetic resonance lineshifts for paramagnetic molecules [25]. The NMR lines must be narrow enough relative to the magnitudes of the lineshifts to permit the measurement of the latter. Thus these lines must not be broadened too much by the relaxation of the proton spins in the presence of the nearby electron spin. This implies that the latter must relax relatively much more rapidly. The proton NMR spectrum of the biphenyl anion at room temperature is shown in Fig. 9.5. The chemical shifts in this spectrum are huge, compared to those found for protons in diamagnetic molecules, and arise from the local magnetic fields generated by each hyperfine interaction. Referring to Fig. 9.5, one notes that there are two lines shifted to the high-field side of the resonance position for diamagnetic molecules. These correspond to a negative value of a_i for two sets of

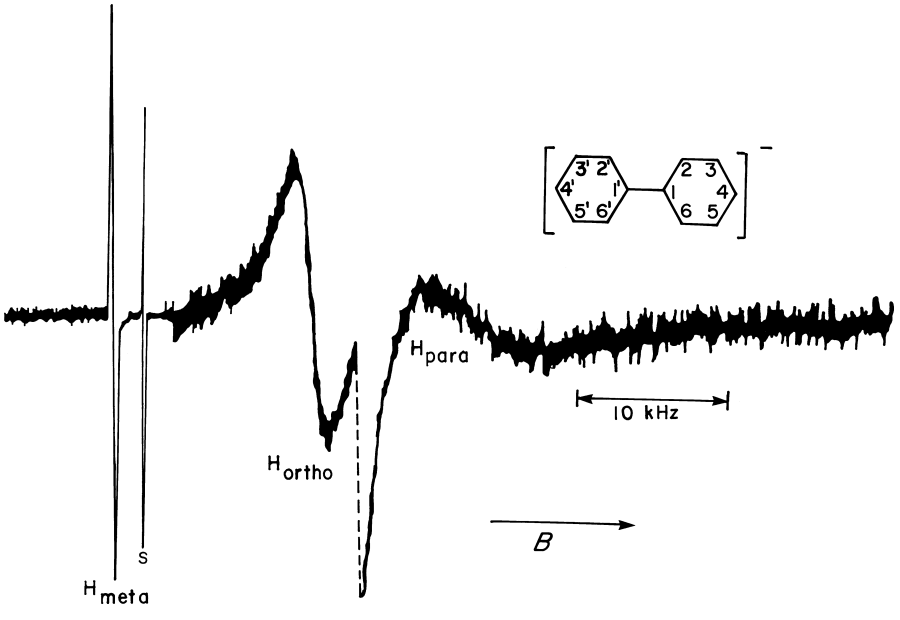

FIGURE 9.5 Proton NMR spectrum at 60 MHz of a 1 M solution of the biphenyl anion, structure (**X**) in diglyme $CH_3—O—(CH_2—CH_2—O—)_2CH_3$ at room temperature. The concentration of neutral biphenyl is negligible. The line S arises from the solvent. Various peaks have been measured with different radiofrequency power, gain and modulation. [After G. W. Canters, E. de Boer, *Mol. Phys.*, **13**, 495 (1967).]

protons in the radical. This result is expected from Eq. 9.6 with a negative value of Q and positive unpaired-electron population at the carbon atom. However, one line is shifted downfield; it must therefore correspond to a *positive* a_i for one set of protons. This result is understandable in terms of the new concept, negative spin density, introduced in the previous section. If proton hyperfine splittings are less than $\sim$0.6 mT, it may be possible to observe paramagnetic chemical shifts ΔB for free radicals in liquid solution [26,27].

The chemical shift ΔB is given by

$$\Delta B = B_i - B_0 = -\frac{g g_e \beta_e{}^2 B_0}{4 g_p \beta_n k_b T} a_i \tag{9.10}$$

for the ith proton, where B_i is the resonance field for the shifted line and B_0 is the field corresponding to the unshifted proton resonance line [28,29]. The derivation of Eq. 9.10 is left to the reader, as Problem 9.2. It follows from Eq. 9.10 that there is a negative (downfield) chemical shift if a_i is positive, and vice versa.

The proton NMR spectrum of the biphenyl anion at room temperature is shown in Fig. 9.5. The chemical shifts in this spectrum are huge, compared to those found for protons in diamagnetic molecules, and arise from the local magnetic fields generated

by each hyperfine interaction. Referring to Fig. 9.5, one notes that there are two lines shifted to the high-field side of the resonance position for diamagnetic molecules. These correspond to a *negative* value of a_i for two sets of protons in the radical. This result is expected from Eq. 9.6 with a negative value of Q and positive unpaired-electron population at the carbon atom. However, one line is shifted downfield; it must therefore correspond to a *positive* a_i for one set of protons. This result is understandable in terms of the new concept, *negative spin density*, introduced in the previous section.

If only one proton is attached to each carbon atom of a conjugated radical and if all π spin densities are positive, the extent (Section 3.5) of the EPR spectrum cannot exceed the value of $|Q|$. For most radicals, the spectral extent does not exceed $\sim$2.7 mT (i.e., $|Q|$). However, for some radicals [e.g., the biphenyl anion (**X**) and the perinaphthenyl radical (**XI**)] the spectral extent is considerably in excess of this value. An extra-large spectral extent can be understood if negative π unpaired-electron populations occur. The normalization condition for unpaired-electron population requires that the *algebraic* sum of all such populations be unity for free radicals. If some populations are negative, then others must be correspondingly more positive. Consequently, the sum of the *absolute values* of the unpaired-electron populations can be greater than unity. Since the spectral extent depends only on the absolute magnitude of the hyperfine splittings, negative spin densities result in a (seemingly) unusually large spectral extent.

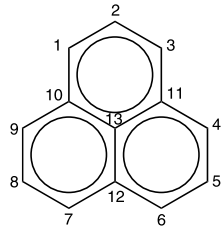

(**XI**) perinaphthenyl radical

In the biphenyl anion spectrum in Fig. 9.5, the line that is shifted downfield must be assigned to positions at which the π spin density is *negative*. One would not have inferred this fact from the spectral extent. However, there are appreciable spin densities at positions that have no attached protons. The magnitude of the shift for the low-field line indicates that this line arises from protons having the *smallest* magnitude of hyperfine splitting. From the solution EPR spectrum, the smallest splitting arises from a set of four equivalent protons. These can be either the protons at positions 2,6,2′,6′ or 3,5,3′,5′ (Fig. 9.5). Molecular-orbital studies indicate that the latter assignment should be made [30].

The HMO theory is too crude to yield negative π-electron spin densities at carbon atoms. With a generalized definition [2] of spin density, distinguishing between spin-α and -β states, more advanced MO schemes do yield these with both signs,

and place non-zero spin density on the protons. Thus, for the latter nuclei, one obtains the relation

$$a_p = \frac{2\mu_0}{3} g\beta_e g_p \beta_n \frac{|\psi|_p{}^2 \rho_p}{\langle \hat{S}_z \rangle} \tag{9.11}$$

to be compared with Eqs. 2.38 and 2.51. Here the wavefunction evaluated at the site of the proton is, of course, *s*-like.

One of the more advanced MO theories, which allows for negative π unpaired-electron populations, is due to McLachlan [30,31]. This theory uses Hückel orbitals as unperturbed functions, and brings in electron interaction and correlation. When there are N carbon atoms in the conjugated system, the expression obtained for the unpaired-electron population at carbon atom t is

$$\rho_t = |c_{mt}|^2 + \lambda \sum_{r=1}^{N} \pi_{rt} |c_{mr}|^2 \tag{9.12}$$

Here c_{mt} is the coefficient of atom t in the mth molecular orbital that contains the unpaired electron. λ is a dimensionless parameter that may be varied to provide a best fit to the spectral extent. It is usually given a value between 1.0 and 1.2. Symbol π_{rt} is the dimensionless mutual atom-atom polarizability defined by

$$\pi_{rt} = -4\beta \sum_{j}^{\text{bonding}} \sum_{k}^{\text{antibonding}} \frac{(c_{jr} c_{kr}{}^*)(c_{jt} c_{kt})}{U_k - U_j} \tag{9.13}$$

The Hückel coefficients c are for atoms r and t in molecular orbitals j and k. U_k and U_j are the Hückel energies of the k and j levels. The summations need not include non-bonding levels, since their effects cancel out in the summations.

9.2.6 Methyl Proton Hyperfine Splittings and Hyperconjugation

Examination of Fig. 9.3 reveals that splittings from some methyl protons exceed those caused by some ring protons. Hence there must be some mechanism that couples the methyl protons to the π system.

An effective model for the coupling mechanism is that of *hyperconjugation* (defined below), which provides a direct link of the methyl hydrogen atoms with electrons in the π system. It is well known that two fragments of a molecule may interact if there is a compatibility in the symmetry properties (and energies) of their wavefunctions. A single $2p_z$ orbital or a π orbital is antisymmetric with respect to the plane of the molecule; that is, it changes sign on reflection in the plane. The atomic orbitals of the three hydrogen atoms may be combined to give

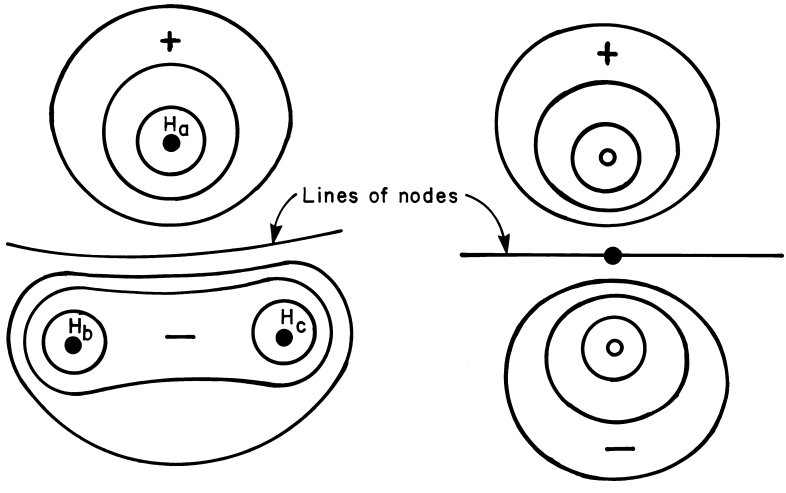

FIGURE 9.6 Schematic representation of a three-hydrogen (3H)-atom molecular orbital of the same symmetry as the p atomic orbital in a conjugated radical. [After C. A. Coulson, *Valence*, Oxford University Press, London, U.K., 1961, p. 362.]

a molecular orbital with the same symmetry as a π orbital. Such a combination is

$$\psi = c_1\phi_1 - c_2(\phi_2 + \phi_3) \tag{9.14}$$

This symmetry is shown schematically in Fig. 9.6. ψ can be considered as a *pseudo-π* orbital. Hence it may be regarded as part of the π system. Because the methyl protons form a part of the π system, the spin density at the protons has the same sign as that on the carbon bonded to the methyl group. It is to be recalled that the hyperfine splitting a_i of a proton i is proportional (Eq. 9.11) to the *square* $|\psi|_p^2$ of the wavefunction at the proton. On CH_3 the protons have identical spin densities, and hence the hyperfine splitting constants from H_a, H_b and H_c of Fig. 9.6 all have the same sign and magnitude.

That the spin density on β protons

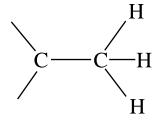

is opposite in sign to that on α protons

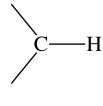

was established by observing an opposite shift of the lines from the two types of protons in a nuclear magnetic resonance experiment [32,33].

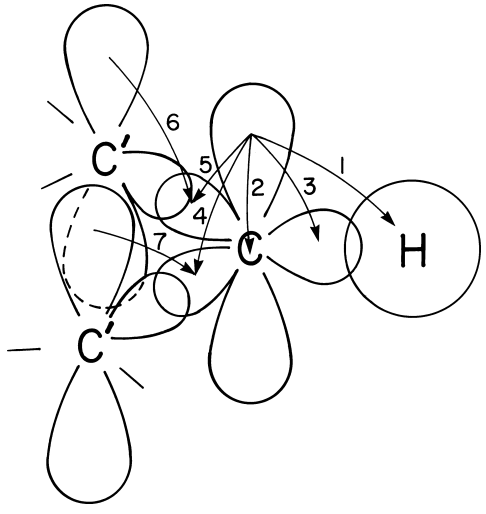

FIGURE 9.7 Spin polarization contributions to the ^{13}C and to the proton hyperfine splittings in a $(C')_2CH$ fragment. The numbered interactions are (1) Q^{H}_{CH}; (2) Q^{C}_{s}; (3) Q^{C}_{CH}; (4,5) $Q^{C}_{CC'}$; (6,7) $Q^{C}_{C'C}$.

9.2.7 Hyperfine Splitting from Nuclei Other than Protons

When isotropic proton hyperfine splittings were considered in Section 9.2.4, it was necessary to consider only the interaction of the π unpaired electron with the σ electrons in one bond (i.e., the C—H bond). However, in the case of nuclei that form part of the framework of a conjugated molecule, the interactions with several bonds must be considered. The hyperfine splittings by ^{13}C are considered first, but the model should generally be applicable to other nuclei, such as ^{14}N, ^{17}O, ^{19}F and ^{33}S [34]. This model is essentially a generalization of the treatment given for the C—H fragment. It has been observed that experimental ^{13}C hyperfine splittings are not simply proportional to the π unpaired-electron population on the same carbon atom. Rather, it is also necessary to include contributions from the populations on neighboring carbon atoms. Figure 9.7 illustrates the several interactions that are present, characterized by appropriate Q parameters. The notation used is as follows. In each Q parameter, the superscript designates the atom giving rise to the hyperfine splitting. In symbol Q^{C}_{s}, the subscript indicates the polarization of the carbon 1*s* electrons by the local π unpaired-electron population. In analogous symbols, the first subscript designates the atom on which the population is contributing to the spin polarization; the two subscripts together indicate the bond that is being polarized.

Consider the $(C')_2CH$ fragment shown in Fig. 9.7. By analogy with the C—H fragment, Q^{C}_{CH} and $Q^{C}_{CC'}$ are expected to be *positive*, whereas $Q^{C}_{C'C}$ and Q^{H}_{CH} should be *negative*. A consideration [34] of the combined contributions leads to the

following relation

$$a_i^{\mathrm{C}} = \left(Q_s{}^{\mathrm{C}} + \sum_{j=1}^{3} Q_{\mathrm{CX}_j}^{\mathrm{C}} \right) \rho_i + \sum_{j=1}^{3} Q_{\mathrm{X}_j\mathrm{C}}^{\mathrm{C}} \rho_j \tag{9.15}$$

where atoms X_j are those bonded to carbon atom $i(\equiv \mathrm{C})$. Quantitative calculations [34] of the spin-polarization constants in Eq. 9.15 yield the following results (in mT):

$$Q_s^{\mathrm{C}} = -1.27, \quad Q_{\mathrm{CH}}^{\mathrm{H}} = +1.95, \quad Q_{\mathrm{CC}'}^{\mathrm{C}} = +1.44 \quad Q_{\mathrm{C}'\mathrm{C}}^{\mathrm{C}} = -1.39$$

Inserting these values into Eq. 9.15, for $(\mathrm{C}')_2\mathrm{CH}$, one obtains (in mT)

$$a_i^{\mathrm{C}} = 3.56\rho_i - 1.39 \sum_j \rho_j \tag{9.16a}$$

where the hydrogen unpaired-electron population has been deemed negligible. Similarly, for a $(\mathrm{C}')_3\mathrm{C}$ fragment, one obtains

$$a_i^{\mathrm{C}} = 3.05\rho_i - 1.39 \sum_j \rho_j \tag{9.16b}$$

These relations are equally applicable to neutral radicals and $+1$ and -1 radical ions. The results of such estimates are displayed in Table 9.4 for the anthracene cation and anion [35]; the sets of experimental and calculated hyperfine splitting constants agree nicely. In this case it was possible to obtain an independent estimate of the π unpaired-electron populations from proton hyperfine splittings, with the aid of Eq. 9.6 and the normalization condition $\sum_i \rho_i = 1$: these are included in Table 9.4. The agreement is very satisfactory, considering that the parameters were calculated

TABLE 9.4 Calculated and Experimental ^{13}C Hyperfine Splitting Parameters and Unpaired-Electron Populations in the Anthracene Cation and Anion [a,b]

	^{13}C Hyperfine Splitting Parameters $\lvert a_i^{\mathrm{C}} \rvert$ (mT)			
Position i	Cation	Anion	Calculated	ρ Experimental [c]
9	+0.848	+0.876	+0.842	0.220
11	−0.450	−0.459	−0.490	−0.021
1	—	+0.357	+0.337	0.107
2	±0.037	−0.025	−0.033	0.054

[a] See structure **VII** in Table 9.3.

[b] From J. R. Bolton, G. K. Fraenkel, *J. Chem. Phys.*, **40**, 3307 (1964).

[c] Calculated from averaged hyperfine splitting constants (Table 9.3) using $Q_{\mathrm{CH}}{}^{\mathrm{H}} = -2.70$ mT and the normalization condition for unpaired-electron populations (Eq. 9.5).

from such an approximate theory. Similar comparison for other radicals show that Eq. 9.15 is widely applicable for ^{13}C splittings in aromatic hydrocarbons.

In nitrogen heterocyclic aromatic molecules, ^{14}N substitutes for carbon atoms; hence one might expect that Eq. 9.15 would also apply to ^{14}N. This is probably correct; however, experience has shown that here the effect of π unpaired-electron populations on neighboring atoms is small. This implies that the factor $Q^{N}_{C'N}$ must be small; certain estimates place it in the range from -0.4 to $+0.4$ mT [36–40]. In view of the small contribution from neighbors, many workers have used a simpler equation similar to Eq. 9.6 for ^{14}N hyperfine splittings.

Hyperfine splittings from ^{17}O [41] and ^{33}S [42] have also been interpreted in terms of an equation similar to Eq. 9.15.

It might be expected that since fluorine substitutes for hydrogen in aromatic molecules, an equation such as Eq. 9.6 would also hold for fluorine hyperfine splittings; that is, if ρ_C is *positive*, one expects that a^F would be *negative*. However, it has been shown conclusively that fluorine hyperfine splittings are *positive* in such molecules [43]. The non-bonding p electrons on the fluorine apparently participate in partial double bonding with the conjugated system to which the fluorine atom is attached; that is, some of the electron density in fluorine p orbitals is delocalized into the π system of the molecule. This electron transfer results in a net π spin density on the fluorine atom, having the same sign as that on the adjacent carbon atom. One expects that the local contribution to a^F (i.e., π unpaired-electron population on F) predominates; this would result in a *positive* fluorine hyperfine splitting constant (see Section 5.3.2.2 for some discussion of this topic).

9.2.8 One-Dimensional Chain Paramagnets

Almost all the systems considered so far have been ones where unpaired electrons are located on isolated relatively small molecules or defects. One-dimensional chain paramagnetic systems represent a class in which unpaired electrons are delocalized over a system of macroscopic dimension. One example is the π system polyacetylene $(CH)_n$ (**XII**), consisting of very long conjugated chains of two types: *cis* and *trans*.

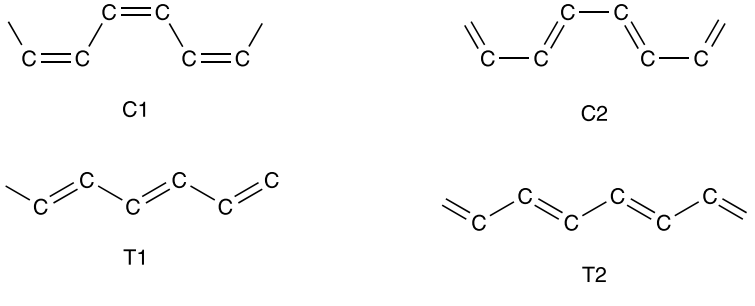

(**XII**) Polyacetylene

In principle, these species should be diamagnetic with double bonds in fixed positions and π electrons delocalized over the chains. In practice, even in highly purified

materials, there are defects that give rise to paramagnetism, and EPR signals are observed [44,45]. These signals tend to be single lines near $g = g_e$; they are thus relatively uninformative.

There is considerable interest, for both *cis* and *trans* materials, in the formation of regions ('domain walls') at which type-1 switches to type-2 bond distribution, with unpaired spins present. Much effort [^{2}H and ^{13}C doping, advanced ENDOR and ESEEM techniques (Chapter 12)] is being brought to bear on this complex system [45,46], especially to discern whether the domain walls are fixed or mobile (solitons). Chemical doping experiments show that polyacetylenes are semiconductors capable of being transformed into excellent electrical conductors that yield EPR signals with dysonian lineshapes (Section 9.6) [44].

A second example of macroscopic π systems involves certain organic molecules that are strong electron donors or acceptors, and can exhibit strong EPR signals under appropriate conditions.

The *p*-phenylenediamines are strong donors. For example, the species forms readily and is called 'Wurster's blue cation' (**XIII**). It exhibits a complex multi-line ^{1}H and ^{14}N hyperfine pattern [47] in aqueous solution, and is known to dimerize to some extent in non-aqueous solutions [48]. In the solid state (e.g., the perchlorate salt), it crystallizes in long parallel one-dimensional chains[5] and undergoes antiferromagnetic spin pairing at low temperatures.

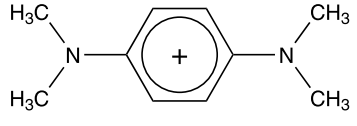

(**XIII**) Wurster's blue cation

Among the strong acceptors, tetracyanoethylene (**XIV**) and tetracyanoquinodimethane (**XV**) have been of considerable interest, since they readily form mono-anion radicals. For instance, pairwise clustering of such species in the crystal form leads to thermally accessible singlet and triplet species, in which the triplet excitation (exciton) is mobile [49]. Many of these materials are semiconductors.

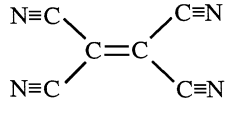

(**XIV**) tetracyanoethylene

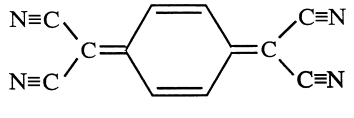

(**XV**) tetracyanoquinodimethane

As an inorganic example, we can cite chains of platinum atoms, bonded directly to each other, but each liganded with various oxygen anions. Thus we deal with one-dimensional (1D) chains of nascent metallic character; these materials are called 'platinum blues'. In one example, a paramagnetic one, there is a mixed chain $Pt(II)_3Pt(III)$ having spin $S = \frac{1}{2}$. EPR studies have yielded principal values $g_\perp = 2.509$ and $g_\parallel = 1.978$, and nicely resolved ^{195}Pt (33.8% natural abundance) hyperfine structure showing that the unpaired electron is highly delocalized along the chain, with all four Pt atoms close to equivalent, with the parallel direction along the mean chain direction **z** [50]. The Pt—Pt bonding can be described in terms of d_{z^2} orbital overlap, in first approximation.

In summary, EPR has played a prominent role in the study of electron spin-spin interactions in these systems. A review [51], up to 1966, is available.

9.3 σ-TYPE ORGANIC RADICALS

For the radicals considered thus far, the unpaired electron is located primarily in a carbon $2p_z$ (or π) orbital. Small isotropic hyperfine couplings ($|a_0| < 100$ MHz) are observed, but these arise primarily from the indirect mechanism described in Section 9.2.3. The nuclei are usually located at or near the nodal plane of the $2p_z$ orbital.

There are a number of known radicals that exhibit proton hyperfine couplings with isotropic components of the order of 150–400 MHz. These couplings are far too large to be explained by the indirect mechanism, and one is forced to conclude that the wavefunction of the unpaired electron has considerable density at the nucleus considered. Thus, the unpaired electron is located primarily in the σ orbital that would normally form a σ bond between that nucleus and some atom (such as hydrogen) absent in the radical. Most σ orbitals have a considerable *s*-orbital component.

In the ethynyl radical C≡C—H, the unpaired electron occupies primarily an orbital pointing outward, that is, one that would be directed toward a second proton in the acetylene molecule. Likewise in the vinyl radical HC═CH_2, the unpaired electron is primarily in an orbital that would attach a hydrogen atom to form the ethylene molecule. Yet another example is the formyl radical HCO, derived from formaldehyde H_2CO, in which the bond angle is thought to be 120° [52]. A closely related radical is FCO.

In each of these cases, the sign of the ^1H (or ^{19}F) hyperfine coupling constant is believed to be positive, arising from a considerable *s* component at the hydrogen (or fluorine) atom. For instance, in the HCO radical, the unpaired-electron population in the 1*s* orbital of hydrogen is approximately 0.27, since the proton hyperfine coupling constant is $0.27 \times 1420 = 384$ MHz [53]. This is an unusually large proton coupling. In terms of resonance structures, it can be assumed to imply considerable presence of H + CO in the ground state.

The magnitude of isotropic ^{13}C hyperfine splittings provides a direct indication of whether there is a significant *s*-orbital contribution on carbon. A pure *s* orbital would yield a ^{13}C hyperfine splitting of ~135 mT (Table H.4). An sp^3 hybrid for a tetrahedral configuration would give 25% of this value. For example, in the π radical

CH_3, the a^C hyperfine splitting constant is only 3.85 mT [54], showing this radical to be close to planar. In the CF_3 radical, $a^C = 27.1$ mT [54]. This large increase in the ^{13}C hyperfine splitting can be explained in terms of a large pyramidal distortion in CF_3. Thus the latter is a σ radical.

It is interesting to compare the isotropic parts of the proton couplings in the formyl (HC═O) and the vinyl radicals. For the latter in a rigid medium, the couplings (in mT) are 1.57 for $H_{(1)}$, 3.43 for $H_{(2)}$ (*cis*), and 6.85 for $H_{(3)}$ (*trans*) [55]. (Problem 10.7 explores the apparent changes in couplings when this radical is observed in liquid solution.) Even the largest value is considerably less than that (13.7 mT) for HCO, which likely has a bond angle of $\sim 125^\circ$. The difference arises from the large variation of coupling constant with bond angle. From the value for $H_{(1)}$ in the vinyl radical, the HCC bond angle is estimated to be $140-150^\circ$.

Hyperfine couplings in σ-type radicals may also exhibit large anisotropy. For example, in FCO, the principal hyperfine matrix components $A(^{19}F)/h$ are 1437.5, 708.2 and 662.0 MHz [55]. Presumably a large spin polarization of the CF bond occurs, arising from configuration interaction between the ground state and a low-lying excited state describable in terms of atomic F and CO.

It is possible to estimate the spin distribution in s radicals by using a molecular-orbital theory, such as the INDO method [2] (which includes all valence-shell atomic orbitals).

9.4 TRIPLET STATES AND BIRADICALS

The triplet state of naphthalene, too, can be discussed in terms of the HMO model. Thus one unpaired electron is in the highest bonding orbital, whereas the other was transferred (Section 6.3.4) from there to the lowest antibonding orbital. In accordance with the pairing theorem, the orbital coefficients of these are equal in magnitude. The unpaired-electron populations obtained experimentally and from various theoretical approaches are listed in Table 9.5. The π-electron populations (Problem 9A.3) sum to 1 (and not 2), consistent with the operation of the Pauli exclusion principle [1, Section 8.5]. These parameters yield a good approximation to the set of proton hyperfine couplings (Section 9.3.4),[6] which are seen to be much the same as those of the naphthalene anion (Section 3.2.2) and cation (Table 9.3), despite the presence here of two unpaired electrons.

It is of interest to calculate the value of D when the two coupled electrons are on the same carbon atom, namely, for CH_2. This hydrocarbon is one of the smallest molecular species with a low-lying triplet state, that is, its $^3B_1$ ground state. It is thus a favorite molecule for theoretical calculations (see Ref. 56 for a summary and also Section 6.3.6.1). Experiment and ab initio calculations agree that CH_2 is non-linear. For a bond angle of 135°, the latter yield $\bar{D} = 0.81\ cm^{-1}$, $\bar{E} = 0.05\ cm^{-1}$ [57]. EPR spectroscopy yields $\bar{D} = 0.76(2)\ cm^{-1}$, when a correction for motional effects is made [58]. In these small molecules, one must be concerned about a possible contribution to D from spin-orbit coupling. In O_2, this contribution

TABLE 9.5 Unpaired-Electron Populations for Naphthalene in Its Lowest Triplet State[a,b]

Source of Data	Spin Population[c]			
	ρ_1	ρ_2	ρ_9	ρ_1/ρ_2
From the anisotropic part of the proton hyperfine splitting	0.219	0.062	−0.063	3.5
From the isotropic part of the proton hyperfine splitting[d]	0.220	—	—	—
From HMO calculations (Problem 9A.3)	0.181	0.069	0	2.6
From advanced MO calculations:				
Amos[e]	0.235	0.048	−0.066	4.89
Pariser[f]	0.168	0.074	0.015	2.27
Goodman and Hoyland[g]	0.198	0.052	0	3.81
Atherton and Weissman[h]	0.220	0.083	−0.106	2.65

[a] See structure **VI** in Table 9.3.
[b] N. Hirota, C. A. Hutchison Jr., P. Palmer, *J. Chem. Phys.*, **40**, 3717 (1964).
[c] For position labeling, see structure **VI**.
[d] Using $Q_{CH}^{H}/h = -66.50 \times 10^6\ s^{-1}$.
[e] A. T. Amos, *Mol. Phys.*, **5**, 91 (1962).
[f] R. Pariser, *J. Chem. Phys.*, **24**, 250 (1962).
[g] L. Goodman, J. R. Hoyland, *J. Chem. Phys.*, **39**, 1068 (1963).
[h] N. M. Atherton, S. I. Weissman, *J. Am. Chem. Soc.*, **83**, 1330 (1961).

is appreciable. However, calculations for CH_2 disclose that the spin-orbit contribution to D and E is small as compared to the spin-spin interaction [57].[7]

The large value of D in H—C—C≡N, notwithstanding the possibility of delocalization in the C≡N group, is probably due to the existence of a negative unpaired-electron population on the central atom of the C—C≡N group. This π system is akin to that of the allyl radical $H_2C(CH)CH_2$ (Problem 9.4 and Appendix 9A). The expected negative populations on the central atom would thus lead to an increased positive population on each outer carbon atom and hence to an increased value of D. Such an effect cannot occur with the H—C—CF_3 molecule listed in Table 6.1. The effect is probably operative in the molecule H—C—C≡C—H also, and assuredly also in N≡C—C—C≡N, where there are five π-electron centers.

Table 6.1 includes the parameters for one nitrene. These species, N—R, are isoelectronic with the carbenes. The parent compound for the nitrenes is N—H. It has been estimated that $\bar{D} = 1.86\ cm^{-1}$ for this fragment [59]. For N—C≡N, the reduction in the D value by delocalization is probably somewhat offset by the enhancement of the positive population on the nitrogen atoms, due to a negative spin density on the carbon.

9.5 INORGANIC RADICALS

The assignment and interpretation of the EPR spectra of inorganic radicals have been a very active field of investigation. It is not possible to give a complete coverage; however, we shall attempt to outline the major features with some examples.

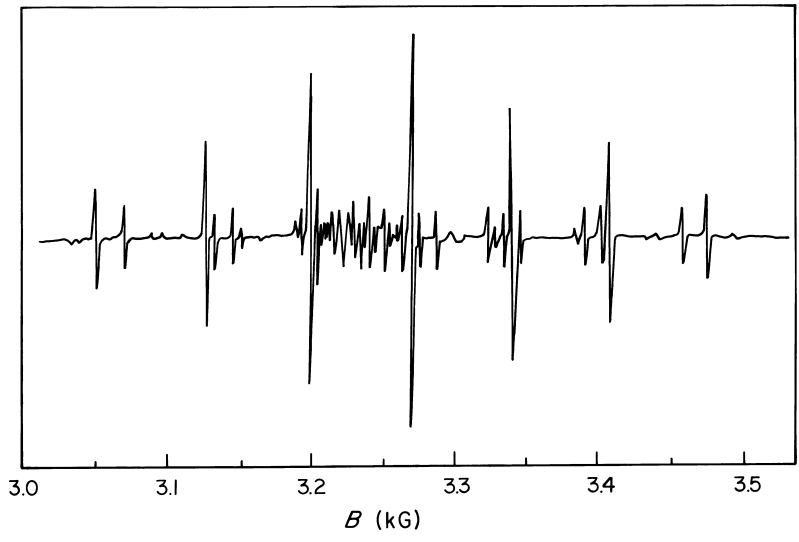

FIGURE 9.8 EPR spectrum of the V_k center (Cl_2^-) in x-irradiated KCl at 77 K with the magnetic field parallel to the [100] direction in the (100) plane, with $v = 9.263$ GHz. [After T. G. Castner, Jr. W. Känzig, *J. Phys. Chem. Solids*, **3**, 178 (1957).]

Identification of Radical Species. As in the case of organic radicals, the values of principal components of hyperfine matrices can provide the major clues in the identification of species resulting from the irradiation of inorganic materials. For example, x irradiation of LiF at 77 K produces (among others) a species that exhibits a 1 2 1 triplet EPR spectrum for $\mathbf{B} \parallel [100]$. Such a pattern implies hyperfine interaction with two nuclei of spin $\frac{1}{2}$. The principal values of the g matrix are $g_X = 2.0234$, $g_Y = 2.0227$ and $g_Z = 2.0031$, indicative of nearly uniaxial symmetry. The hyperfine splitting shows uniaxial behavior, with $a_{\parallel} = 88.7$ mT and $a_{\perp} = 5.9$ mT [60]. The species responsible is undoubtedly the F_2^- ion (V_K center). If the experiment is done with KCl, the spectra (Fig. 9.8) from the molecular ions $(^{35}Cl—^{35}Cl)^-$, $(^{35}Cl—^{37}Cl)^-$ and $(^{37}Cl—^{37}Cl)^-$ provide redundant and incontrovertible (and redundant) identification that the center here is Cl_2^-. Interpretation of Fig. 9.8 is left as a problem for the reader.

In other cases the appearance of hyperfine structures is not sufficient to provide a positive identification. For example, γ-irradiated KNO_3 exhibits the EPR spectrum shown in Fig. 9.9. There are at least three radical species, each of which contains a nitrogen atom, as evidenced by the triplet hyperfine splittings. However, the assignment to specific radicals requires further information. The reasonable possibilities can be listed as NO_2, NO_2^{2-}, NO_3, and NO_3^{2-}. The experimental results for the hyperfine and g matrix principal values are listed in Table 9.6.

The identification requires a knowledge of the theoretical predictions of the structure and orbital sequence in each radical; in addition, one requires information from

FIGURE 9.9 Spectra of radicals obtained on γ irradiation of KNO_3. Species 1 (lines α, β and γ) has been assigned as the NO_2 radical. Species 2 (lines a, b and c) has been assigned as the NO_3^{2-} radical. [After R. Livingston, H. Zeldes, *J. Chem. Phys.*, **41**, 4011 (1964).]

studies of these radicals in other host matrices. In various hosts, NO_2 exhibits a ^{14}N hyperfine coupling with little anisotropy and an isotropic hyperfine coupling of about 150 MHz [61]. The small anisotropy arises from the fact that NO_2 is usually rotating about its two-fold axis, even in a solid. *Fixed* NO_2 exhibits

TABLE 9.6 Hyperfine and g Matrices for Radical Species Found in γ-Irradiated KNO_3

Species	g Components	^{14}N Hyperfine Components (MHz)
1	$g_\parallel = 2.006$[a]	$A_\parallel/h = 176$[a]
	$g_\perp = 1.996$	$A_\perp/h = 139$
2	$g_\parallel = 2.0031$[b]	$A_\parallel/h = 12.08$[b]
	$g_\perp = 2.0232$	$A_\perp/h = 9.80$
3	$g_\parallel = 2.0015$[a]	$A_\parallel/h = 177.6$[a]
	$g_\perp = 2.0057$	$A_\perp/h = 89.0$

[a] H. Zeldes, "Paramagnetic Species in Irradiated KNO_3", in *Paramagnetic Resonance*, Vol. 2, W. Low, Ed., Academic Press, New York, NY, U.S.A., 1963, p. 764.
[b] R. Livingston, H. Zeldes, *J. Chem. Phys.*, **41**, 4011 (1964).

considerable anisotropy. The large hyperfine coupling arises from the fact that the unpaired electron is located primarily in a non-bonding orbital on nitrogen. The g matrix is virtually isotropic, with $g_{\text{iso}} \approx 2.000$. Comparison with Table 9.6 indicates that species 1 is probably the NO_2 radical.

In NO_3 (the symmetric isomer; D_{3h}) the unpaired electron is located in an orbital composed largely of non-bonding oxygen p orbitals lying in the plane of the molecule. Thus the nitrogen hyperfine coupling is expected to be very small. Examination of the results in Table 9.6 suggests that species 2 may be this NO_3 radical.

Species 3 exhibits considerable isotropic and anisotropic hyperfine interaction. NO_3^{2-} is a reasonable possibility, since this ion is expected to be not quite planar [62], that is, a slightly distorted π-type radical. The distortion would introduce some s character into the orbital of the unpaired electron and thus account for the large isotropic hyperfine coupling ($\sim$120 MHz).

Structural Information. When a radical species has been identified, the g and hyperfine matrices can provide considerable information about the detailed geometric and electronic structure of the radical. The NO_2 radical (observed in $NaNO_2$ [63]) is an excellent example. From Table H.4 one notes that a single electron in a $2s$ orbital on a free nitrogen atom would give rise to an isotropic hyperfine coupling of 1540 MHz. From the observed value of $A_0/h = 151$ MHz, the unpaired-electron population in the nitrogen $2s$ orbital is computed to be $\rho_s = \frac{151}{1540} = 0.10$. Similarly, from the maximum value in the anisotropic hyperfine matrix, the population in the nitrogen $2p_x$ orbital is computed to be $\rho_p = \frac{12}{48} = 0.25$. Hence the $2p/2s$ ratio is 2.5. A simple consideration of orbital hybridization suggests that the bond angle is between 130° and 140°. This is in good agreement with gas-phase vibrational analysis [64] and microwave results (134°) [65]. Presumably, the unpaired-electron populations for the nitrogen $2p$ and $2s$ orbitals do not add up to unity because there is some population in $2p$ orbitals on the oxygen atoms.

When isotropic hyperfine couplings are small, as for species B in Table 9.6, one must beware of interpreting these in terms of a percentage of s character in the orbital of the unpaired electron. The indirect mechanism leading to isotropic hyperfine coupling (Section 9.2.3) may give the major contribution. Generally, if $|\rho_s| < 0.05$ as computed above, then an interpretation in terms of a bond angle is dubious.

It is interesting to compare the EPR results for isoelectronic series of radicals. Table 9.7 contains the data for the ClO_3, SO_3^-, and PO_3^{2-} radicals, as well as for the NO_2 and CO_2^- radicals. It is clear that as the atomic number of the central atom decreases, the tetratomic radicals become more pyramidal (as evidenced by the decreased ratio ρ_p/ρ_s); the triatomic radicals become more bent.

As a final example of inorganic radicals, we cite the EPR of adsorbed oxygenic species [66]. The $S = \frac{1}{2}$ ions O^-, O_2^- and O_3^- on the surfaces of various materials all show characteristic spectra, corroborated with the help of ^{17}O enrichment, and undergo chemical interconversions of catalytic interest.

TABLE 9.7 Comparison of the EPR Data for Central Atoms of Some Isoelectronic ($S = \frac{1}{2}$) Radicals

		g			Hyperfine (MHz)				Unpaired-Electron Populations				
Radical	Host	g_{XX}	g_{YY}	g_{ZZ}	T_{XX}/h	T_{YY}/h	T_{ZZ}/h	A_0/h	ρ_s	ρ_p	ρ_p/ρ_s	$\rho_s + \rho_p$	Reference
$^{35}ClO_3$	$KClO_4$	2.0132	2.0132	2.0066	−40.5	−40.5	81	342	0.076	0.34	4.5	0.42	*a*
$^{33}SO_3^-$	$K_2CH_2(SO_3)_2$	—	—	—	−37	−39	75	353	0.13	0.49	3.8	0.62	*b*
$^{31}PO_3^{2-}$	$Na_2HPO_3 \cdot 5H_2O$	2.001	2.001	1.999	−148	−148	297	1660	0.16	0.53	3.3	0.69	*c*
$^{14}NO_2$	$NaNO_2$	2.0057	2.0015	1.9910	−22.3	37.0	−14.8	153	0.099	0.44	4.4	0.54	*d*
$^{13}CO_2^-$	NaO_2CH	2.0032	2.0014	1.9975	−32.0	78.0	−46.0	468	0.14	0.66	4.7	0.80	*e*

[a] P. W. Atkins, J. A. Brivati, N. Keen, M. C. R. Symons, P. A. Trevalion, *J. Chem. Soc.*, 4785 (1962).
[b] G. W. Chantry, A. Horsfield, J. R. Morton, J. R. Rowlands, D. H. Whiffen, *Mol. Phys.*, **5**, 233 (1962).
[c] A. Horsfield, J. R. Morton, D. H. Whiffen, *Mol. Phys.*, **4**, 475 (1961).
[d] H. Zeldes, R. Livingston, *J. Chem. Phys.*, **35**, 563 (1961).
[e] D. W. Ovenall, D. H. Whiffen, *Mol. Phys.*, **4**, 135 (1961). See also T. A. Vestad, H. Gustafsson, A. Lund, E. O. Hole, E. Sagstuen, *Phys. Chem. Chem. Phys.*, **6**, 3017 (2004).

9.6 ELECTRICALLY CONDUCTING SYSTEMS

Electrically conducting systems represent another example (see Section 9.2.8) of interacting electrons; in this case the cooperativity extends over the entire macroscopic sample. We consider metals, metal ammonia and amine solutions, semiconductor, and graphitic materials. The analysis of EPR lineshapes and linewidths can in principle yield information about the electrical conductivity, conduction-electron g factor and spin relaxation time, the electron state density on the Fermi energy surface and carrier diffusion parameters. Frequently, especially in solids, mobile electrons are called 'itinerant'.

9.6.1 Metals

Metals may be visualized as a matrix of fixed cations in a sea of highly delocalized (conduction) electrons; as they are highly mobile, they are able to interact with each

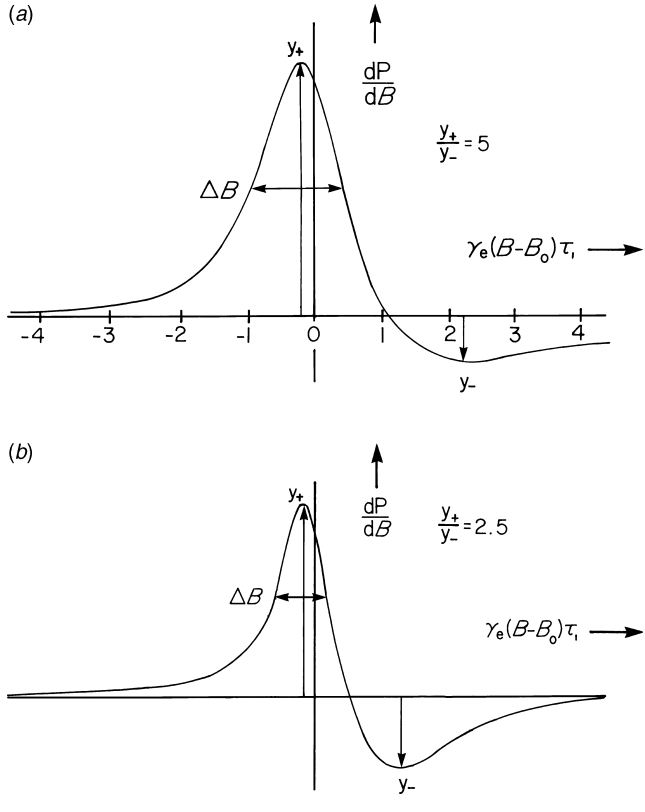

FIGURE 9.10 (*a*) First derivative of the ideal dysonian absorption line in the X-band region; (*b*) typical first-derivative EPR spectrum observed in colloidal samples of Na(s), with mean particle diameter small compared to the skin depth. Horizontal scale is not the same as in (*a*). [After F. Vescial, N. S. VanderVen, R. T. Schumacher, *Phys. Rev.*, **134**, A1286 (1964).]

other. EPR signals are observed [67]; however, only the layers near the surface contribute, since the excitation field $\mathbf{B}_1$ penetrates only a short distance ($\sim$1 μm) into the metal (skin effect).

The magnetic susceptibility in metals has a diamagnetic component due to the circulation of electrons in the field **B**. This is opposed by the normal paramagnetic component due to the unpaired electrons. The *g* factors of the observed EPR spectra are close to g_e. For example, in sodium metal, $g - g_e = 9.7(3) \times 10^{-4}$ in both the liquid and solid phases [68]. The EPR lineshape typically is asymmetric (Fig. 9.10), arising from a mixture of absorption and dispersion effects. This admixture arises because the electron diffusion relative to the surface occurs in times that typically are long compared to the spin-relaxation times, as explained by Dyson and others [69,70].

It has been possible to study *S*-state ions in metals [71], and thus to learn details of the interaction between the conduction electrons and the inserted spin probes (gadolinium ions). The observed *g* shifts (2.01 – 1.88) correlate nicely with certain properties of the pure alloys used as solvents.

9.6.2 Metals Dissolved in Ammonia and Amine Solutions

When alkali or alkaline-earth metals (M) are dissolved in liquid ammonia or amines, ionization takes place to produce metal cations and solvated electrons. The latter (blue color when dilute in liquid NH_3) exhibit very sharp EPR lines (width 0.002 mT!) with $g = 2.0012(2)$, independent of concentration ($<$1 M) and of cation M^+ [72–74].

In concentrated solutions (bronze in color), the electronic conductivity becomes metallic, rather than electrolytic, and the EPR line broadens, becoming dysonian in shape [74]. Furthermore, solid cubic complexes $M(NH_3)_x$ can be isolated [e.g., $Li(NH_3)_4$ [75]] that exhibit EPR lines with dysonian shapes characteristic of normal metallic behavior [76].

Dilute solutions of metals in amines exhibit EPR spectra with resolved ^{14}N hyperfine splittings, which give some insight into the structure and dynamics of the interaction of the electron with the surrounding solvent molecules [77].

With crown ethers, such as 18C6 (**XVI**) (inert ligands capable of encapsulating alkali cations), it is possible to isolate stable electrides [e.g., $Cs^+(18C6)_2e^-$] containing

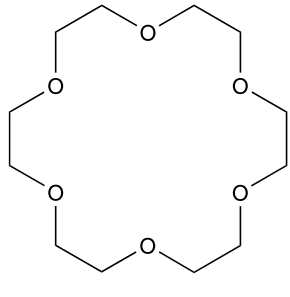

(**XVI**) 18C6 crown ether

close to a unity stoichiometric ratio of electron anions to metal cations. The crystals exhibit a single dysonian line at $g \approx g_e$ (linewidth 0.05 mT) down to 3 K [77,78]. The temperature dependence of the electrical conductivity suggests that the material is a semiconductor with a band-gap energy of 0.9(1) eV.

9.6.3 Semiconductors

Semiconductors, like insulators, have virtually continuous electronic energy bands, derived from orbitals based on all atoms in the crystal. The highest occupied band (valence band) is virtually filled with electrons and is separated from the next virtually unoccupied band (conduction band) by an energy gap (band-gap) that has few or no energy levels. In insulators the band gap is very large (>4 eV), so that thermal excitation of electrons from the valence band to the conduction band is rare. In semiconductors the band gap is smaller (1–3 eV), so that electron (and hole) conductivity, arising from promotion of electrons between these two bands, is possible at moderate temperatures. This conductivity may be enhanced greatly by doping with appropriate donors (*n*-type) or acceptors (*p*-type), which leads to formation of paramagnetic species.[8]

EPR has proved to be an important tool in the study of semiconductors, particularly in identifying and elucidating the structure of point defects and impurity ions. For example, the tetrahedral structure of solid Si can be damaged by electron irradiation, generating defects (V^+, V^0 and V^-) at which electrons are trapped next to Si atoms with 'dangling' bonds [81–83]. The neutral vacancy (V^0) has four interacting dangling bonds that interact to produce spin pairing and thus is diamagnetic. The V^- and V^+ species have $S = \frac{1}{2}$ and exhibit EPR spectra, often with resolvable ^{29}Si hyperfine splittings.

Center V^+ exhibits an EPR spectrum featuring three equally intense prominent peaks, each flanked by weaker ^{29}Si hyperfine doublets [74,84]. On applying uniaxial stress to the crystal, one can alter the relative intensities of the three peaks (Fig. 9.11). The explanation for the triplet is that any one of three energy-equivalent distortions occurs at each vacancy site, differing in the location of the one-electron bond and the two-electron bond formed between the four tetrahedral silicon neighbors. External stress redistributes these bond configurations among each other.

The mixed semiconductors (III–V or II–VI) have also been widely studied by EPR/ENDOR. The anion anti-site center in *p*-type GaP [85] is an example of a center in which a group-V atom occupies a group-III atom site, forming a "double donor". For example, the center $P^{4+}(P^{3-})_4$ exhibits an EPR spectrum (Fig. 9.12) with $g = 2.007(3)$, consisting of an isotropic hyperfine doublet ($a_0 = 103$ mT) arising from the central P ion; each of these lines is split into an (anisotropic) 1 : 4 : 6 : 4 : 1 quintet (~9 mT) from interaction with the four tetrahedrally disposed P neighbors [85]. A superior technique for investigating such defects, and others in semiconductors, features optical detection of EPR and ENDOR (Chapter 12).

For example, a 1992 study [86] reports detection of the microwave-modulated luminescence (at 0.8 eV) from the first-neighbor ^{31}P shell of the phosphorus antisite

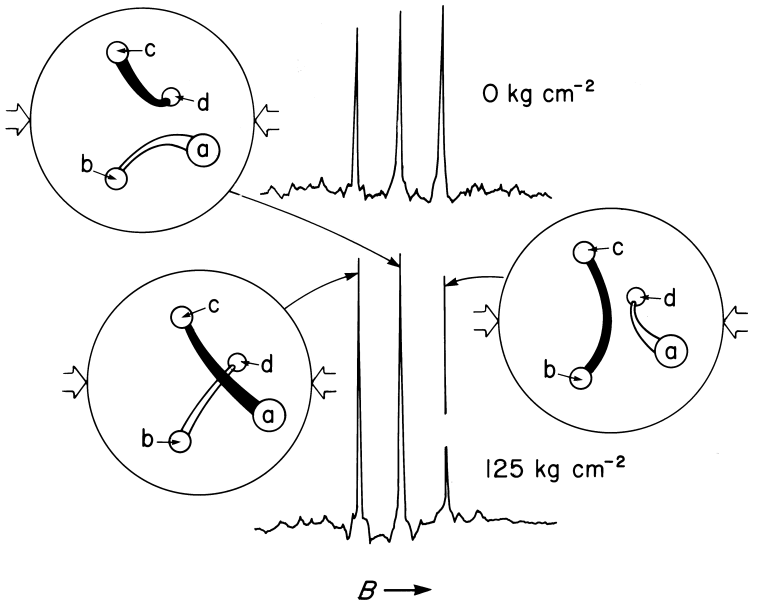

FIGURE 9.11 Changes in the 20-GHz EPR spectrum of the silicon vacancy center V^+ (at 4 K) under compressional stress. The insets sketch the defect bonding pattern corresponding to each line. Here **B** ∥ [100]. The stress was applied along [100]. [After G. D. Watkins, *J. Phys. Soc. Jpn.*, 18, Suppl. **2**, 22 (1963).]

in zinc-doped InP, yielding $|A_\parallel|/h = 368.0(5)$ and $|A_\perp|/h = 247.8(5)$ MHz for each of the four nuclei.

Numerous other magnetic defects—for example, clusters of vacancies, interstitials, and transition ions—also occur in semiconductors, but these cannot be discussed here.

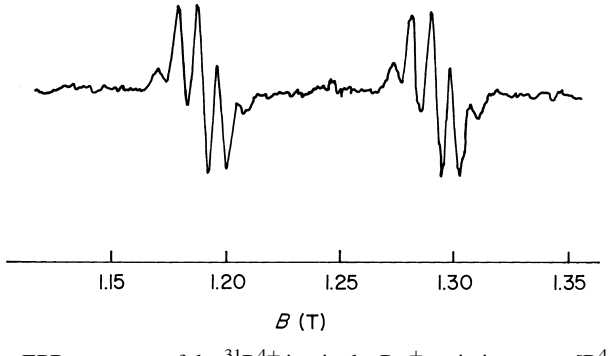

FIGURE 9.12 EPR spectrum of the $^{31}P^{4+}$ ion in the P_{Ga}^+ anti-site center $[P^{4+}(P^{3-})_4]$ in the II–V semiconductor GaP (34.8 GHz, **B** ∥ [100], 20 K). [After U. Kaufmann, J. Schneider, *Festkörperprobleme*, **20**, 87 (1980).]

Clusters of molecules also show semiconductor properties. An interesting example is lithium phthalocyanine (LiPc) (**XVII**), in which the π-radical rings

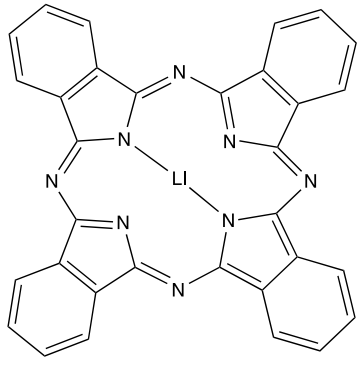

(**XVII**) lithium phthalocyanine

stack linearly with the Li atoms superimposed. The EPR spectrum of the solid consists of an exchange-narrowed sharp line ($\Delta B_{pp} \approx 0.005$ mT) at $g = 2.0015$ [87,88]. This broadens dramatically as a result of exchange interactions when O_2 (Section 10.5.3.1), diffusing rapidly through the channels in the crystal, is admitted (and does so reversibly). The substance is chemically stable and offers a sensitive and rapid means of measuring O_2 concentrations in solutions by means of EPR.

9.6.4 Graphitic Compounds

Graphitic intercalation compounds are distinct in that they are highly anisotropic. A comprehensive review of the status of the conduction EPR field of these conducting 'metallic' materials became available in 1997 [89].

9.7 TECHNIQUES FOR STRUCTURAL ESTIMATES FROM EPR DATA

Despite the ultimate need for complex large-scale numerical modeling, various more or less empirical but relatively simple techniques have been developed to attain structural information from the electron-spin electron-spin interaction parameters (D, J, set of B_4^m discussed in Section 9.7.2).

9.7.1 The Newman Superposition Model

This empirical technique [90–92], applied mostly to transition ions embedded in a symmetric crystal structure (e.g., in a mineral), can describe the electronic quadrupole matrix **D** in terms of additive uniaxial crystal-field contributions from the nearest-neighbor ions. It can give information about the coordination number, ligands and local symmetry, and has most often been applied to S-state ions (Mn^{2+}, Fe^{3+} and Gd^{3+}) in oxides and halides.

The Newman model postulates that

$$D = \frac{1}{2} D_0 \sum_i (3\cos^2 \theta_i - 1)\left(\frac{R_D}{R_i}\right)^{t_D} \tag{9.17}$$

for metal ion M and ligand type X. The sum is over the nearest-neighbor ligands (all of the same type), polar angle θ_i gives the direction between ligand X_i and axis **z** of a cartesian set fixed at M, and the distance between M and X_i is R_i. Parameters $D_0(M, X, R_0)$, R_D and t_D are evaluated empirically; typically, the reference distance is $0.19 \leq R_D \leq 0.21$ nm and $t_D = 8 \pm 1$.[9] For parameter E, an equation differing from Eq. 9.17 only in the form of the angular factor is appropriate.

For systems MnX_6^{4-} with X = Cl, Br and I, studies reveal that parameter D_0 increases monotonically with increasing covalence of the Mn—X bonds [94]. Its complex behavior depends, for instance, on local distortions.

As a second example, we cite the good success of the Newman model in the interpretation of the S^2 and S^4 parameters for Fe^{3+} in a cation site of Li_2O, where two neighbor sites appear to be Li^+ vacancies [95]. However, the model is none too successful in some same cases [96].

9.7.2 The Pseudo-cube Method

The fourth-order terms, that is, measured coefficients of spin-hamiltonian terms quartic in the components of (Section 6.6 and Eqs. 8.17), are even more sensitive than those (i.e., **D**) quadratic in $\hat{S}$. They are found to be useful, despite the fact that they are seldom available with the same accuracy as **D**, in learning about the location of S-state ions and their local environment.

The method of analysis, developed by Michoulier and Gaite [97,98], depends on transforming the fourth-order measured parameters to various rotated coordinate frames (other than the lab crystal frame) until one is found exhibiting the highest local symmetry around the paramagnetic ion being investigated. Various criteria for this have been developed. For example, the sites of Fe^{3+} ions in $KTiOPO_4$ can be identified uniquely as being type Ti(1) rather than Ti(2), by means of the pseudo-cube method [99].

9.7.3 Distances from Parameter D

In triplet-state systems, some rough estimates of interelectron distances are available from the principal values of **D**, that is, from D and E that depend on the mean distance (i.e., on r^{-3}) between the two electrons with parallel spins. In particular, from Eqs. 6.15 and 6.25, one has (see also Eq. 6.41)

$$D = \frac{3\mu_0}{16\pi}(g\beta_e)^2\left\langle \frac{r^2 - 3Z^2}{r^5} \right\rangle \tag{9.18a}$$

$$E = \frac{3\mu_0}{16\pi}(g\beta_e)^2\left\langle \frac{Y^2 - X^2}{r^5} \right\rangle \tag{9.18b}$$

where X, Y, Z are the components of the interelectron vector expressed in the principal-axis system. Thus experimental values (e.g., obtained from Eqs. 6.32) can provide information about the spatial disposition of the two electrons, if the averages over the electron positions in Eqs. 9.18 can be modeled. This analysis is valid only if the interaction is predominantly dipolar in nature, that is, if there is no significant contribution from spin-orbit coupling to **D**.

9.7.4 Eatons' Interspin-Distance Formula

It has proved possible to extract mean distances r between spin-$\frac{1}{2}$ centers via the simple formula

$$\frac{\mathcal{A}(\Delta M_S = \pm 2)}{\mathcal{A}(\Delta M_S = \pm 1)} = k_r r^{-6} \tag{9.19}$$

where the left side contains the ratio of the integrated areas (under the absorption curve) for the two types of transitions possible (Section 6.3), corrected for any hyperfine effects present. The proportionality factor k_r is obtainable by a suitable procedure [100,101]. The recommended value is $k_r = 1.95 \times 10^{-3}\ \text{nm}^6$. This method is valid when the dipole-dipole interaction dominates over anisotropic exchange, typically for $r > 0.4\ \text{nm} = 4\ \text{Å}$. The method has been applied, for example, to obtain r for an interacting Cu^{2+} $(3d^9)$—nitroxyl spin-labeled species [100].

9.7.5 Summary

EPR is rapidly becoming an excellent tool for discerning atom positions, as well as bond lengths and directions, in paramagnetic species. Because of its sensitivity, this technique can furnish such information where non-spectroscopic methods (e.g., x-ray diffraction) fail. A recent journal issue is devoted to this topic [102].

REFERENCES

1. A. Carrington, A. D. McLachlan, *Introduction to Magnetic Resonance*, Harper & Row, New York, NY, U.S.A., 1967, p. 81.
2. J. A. Pople, D. L. Beveridge, P. A. Dobosh, *J. Am. Chem. Soc.*, **90**, 4201 (1968).
3. D. L. Tierney, H. Huang, P. Martásek, L. J. Roman, R. B. Silverman, B. M. Hoffman, *J. Am. Chem. Soc*., **122**, 7869 (2000).
4. M. Weissbluth, *Atoms and Molecules*, Academic press, New York, NY, U.S.A., 1978.
5. D. H. Levy, R. J. Myers, *J. Chem. Phys.*, **41**, 1062 (1964).
6. H. M. McConnell, *J. Chem. Phys.*, **24**, 764 (1956).
7. H. M. McConnell, D. B. Chesnut, *J. Chem. Phys.*, **28**, 107 (1958).
8. S. I. Weissman, *J. Chem. Phys.*, **25**, 890 (1956).
9. R. Bersohn, *J. Chem. Phys.*, **24**, 1066 (1956).

10. T. Cole, C. Heller, H. M. McConnell, *Proc. Natl. Acad. Sci. U.S.A.*, **45**, 525 (1959).
11. R. W. Fessenden, R. H. Schuler, *J. Chem. Phys.*, **39**, 2147 (1963).
12. J. R. Bolton, A. Carrington, *Mol. Phys.*, **4**, 497 (1961).
13. R. G. Lawler, J. R. Bolton, G. K. Fraenkel, T. H. Brown, *J. Am. Chem. Soc.*, **86**, 520 (1964).
14. A. D. McLachlan, *Mol. Phys.*, **2**, 271 (1959); **5**, 51 (1962).
15. J. Koutecky, *J. Chem. Phys.*, **44**, 3702 (1966).
16. J. P. Colpa, J. R. Bolton, *Mol. Phys.*, **6**, 273 (1963).
17. J. R. Bolton, *J. Chem. Phys.*, **43**, 309 (1965).
18. A. J. Stone, *Proc. Roy. Soc.* (*London*), **A271**, 424 (1963).
19. A. J. Stone, *Mol. Phys.*, **6**, 509 (1963); **7**, 311 (1964).
20. R. A. Rouse, M. T. Jones, *J. Magn. Reson.*, **19**, 294 (1975).
21. R. E. Moss, A. J. Perry, *Mol. Phys.*, **22**, 789 (1971).
22. M. T. Jones, T. C. Kuechler, S. Metz, *J. Magn. Reson.*, **10**, 149 (1973).
23. M. Weissbluth, "The Triplet State in Molecular Biophysics", in *Molecular Biophysics*, B. Pullman, M. Weissbluth, Eds., Academic Press, New York, NY, U.S.A., 1965, pp. 694–696.
24. R. Skinner, J. A. Weil, *Am. J. Phys.*, **57**, 777 (1989).
25. R. S. Drago, *Physical Methods of Chemistry*, Saunders, Philadelphia, PA, U.S.A., 1977, Chapter 12.
26. E. de Boer, C. MacLean, *Mol. Phys.*, **9**, 191 (1965).
27. K. H. Hausser, H. Brunner, J. C. Jochims, *Mol. Phys.*, **10**, 253 (1966).
28. H. M. McConnell, C. H. Holm, *J. Chem. Phys.*, **27**, 314 (1957).
29. D. R. Eaton, W. D. Phillips, "Nuclear Magnetic Resonance of Paramagnetic Molecules", in J. S. Waugh, Ed., *Advances in Magnetic Resonance*, Vol. 1, Academic Press, New York, NY, U.S.A., 1965.
30. A. D. McLachlan, *Mol. Phys.*, **3**, 233 (1960).
31. See also L. Salem, *The Molecular Orbital Theory of Conjugated Systems*, Benjamin, New York, NY, U.S.A., 1966, Chapter 5.
32. A. Forman, J. N. Murell, L. E. Orgel, *J. Chem. Phys.*, **31**, 1129 (1959).
33. D. Lazdins, M. Karplus, *J. Am. Chem. Soc.*, **87**, 920 (1965).
34. M. Karplus, G. K. Fraenkel, *J. Chem. Phys.*, **35**, 1312 (1961).
35. J. R. Bolton, G. K. Fraenkel, *J. Chem. Phys.*, **40**, 3307 (1964).
36. R. L. Ward, *J. Am. Chem. Soc.*, **84**, 332 (1962).
37. J. C. M. Henning, C. de Waard, *Phys. Lett.*, **3**, 139 (1962).
38. D. H. Geske, G. R. Padmanabhan, *J. Am. Chem. Soc.*, **87**, 1651 (1965).
39. J. C. M. Henning, *J. Chem. Phys.*, **44**, 2139 (1966).
40. C. L. Talcott, R. J. Myers, *Mol. Phys.*, **12**, 549 (1967).
41. M. Broze, Z. Luz, B. L. Silver, *J. Chem. Phys.*, **46**, 4891 (1967).
42. P. D. Sullivan, *J. Am. Chem. Soc.*, **90**, 3618 (1968).
43. D. R. Eaton, A. D. Josey, W. D. Phillips, R. E. Benson, *Mol. Phys.*, **5**, 407 (1962).

44. I. B. Goldberg, H. R. Crowe, P. R. Newman, A. J. Heeger, A. G. MacDiarmid, *J. Chem. Phys.*, **70**, 1132 (1979).
45. S. Roth, H. Bleier, *Adv. Phys.*, **36**, 385 (1987).
46. E. J. Hustedt, H. Thomann, B. H. Robinson, *J. Chem. Phys.*, **92**, 978 (1990).
47. J. R. Bolton, A. Carrington, J. dos Santos-Veiga, *Mol. Phys.*, **5**, 615 (1962).
48. A. Kawamori, A. Honda, N. Joo, K. Suzuki, Y. Ooshika, *J. Chem. Phys*., **44**(11), 4364 (1966).
49. M. T. Jones, D. B. Chesnut, *J. Chem. Phys.*, **38**, 1311 (1963).
50. P. Arrizabalaga, P. Castan, M. Geoffroy, J.-P. Laurent, *Inorg. Chem*., **24**, 3656 (1985).
51. P. L. Nordio, Z. G. Zoos, H. M. McConnell, *Annu. Rev. Phys. Chem.*, **17**, 237 (1966).
52. F. J. Adrian, E. L. Cochran, V. A. Bowers, *J. Chem. Phys.*, **36**, 1661 (1962).
53. F. J. Adrian, E. L. Cochran, V. A. Bowers, *J. Chem. Phys.*, **43**, 462 (1965).
54. R. W. Fessenden, R. H. Schuler, *J. Chem. Phys.*, **43**, 2704 (1965).
55. E. L. Cochran, F. J. Adrian, V. A. Bowers, *J. Chem. Phys.*, **40**, 213 (1964).
56. J. F. Harrison, *Acc. Chem. Res.*, **7**, 378 (1974).
57. S. R. Langhoff, *J. Chem. Phys.*, **61**, 3881 (1974).
58. E. Wasserman, R. S. Hutton, V. J. Kuck, W. A. Yager, *J. Chem. Phys.*, **55**, 2593 (1971).
59. J. A. R. Coope, J. B. Farmer, C. L. Gardner, C. A. McDowell, *J. Chem. Phys.*, **42**, 54 (1965).
60. T. G. Castner Jr., W. Känzig, *J. Phys. Chem. Solids*, **3**, 178 (1957).
61. P. W. Atkins, M. C. R. Symons, *J. Chem. Soc.*, 4794 (1962).
62. A. D. Walsh, *J. Chem. Soc.*, 2296 (1953).
63. H. Zeldes, R. Livingston, *J. Chem. Phys.*, **35**, 563 (1961).
64. G. E. Moore, *J. Opt. Soc. Am.*, **43**, 1045 (1953).
65. G. R. Bird, *J. Chem. Phys.*, **25**, 1040 (1956).
66. J. H. Lunsford, *Catal. Rev.*, **8**, 135 (1973).
67. R. N. Edmonds, M. R. Harrison, P. P. Edwards, *Annu. Rep. Prog. Chem.*, **C82**, 265 (1985).
68. R. A. B. Devine, R. Dupree, *Philos. Mag.*, **21**, 787 (1970).
69. F. J. Dyson, *Phys. Rev.*, **98**, 349 (1955).
70. G. Feher, A. F. Kip, *Phys. Rev.*, **158**, 225 (1967).
71. M. Peter, D. Shaltiel, J. H. Wernick, H. J. Williams, J. B. Mock, R. C. Sherwood, *Phys. Rev*., **126**(4), 1395 (1962).
72. C. A. Hutchison Jr., R. C. Pastor, *J. Chem. Phys.*, **21**, 1959 (1953).
73. T. P. Das, *Adv. Chem. Phys.*, **4**, 303 (1962).
74. R. S. Alger, *Electron Paramagnetic Resonance Techniques and Applications*, Wiley-Interscience, New York, NY, U.S.A., 1968, Section 6.3.
75. W. S. Glaunsinger, M. J. Sienko, *J. Chem. Phys.*, **62**, 1873, 1883 (1975).
76. J. L. Dye, Prog. *Inorg. Chem.*, **32**, 327 (1984).
77. P. P. Edwards, *J. Solution Chem.*, **14**, 187 (1985); *J. Phys. Chem.*, **88**, 3772 (1984).
78. D. Issa, A. Ellaboudy, R. Janakiraman, J. L. Dye, *J. Phys. Chem.*, **88**, 3847 (1984).

79. F. C. Rong, W. R. Buchwald, E. H. Poindexter, W. L. Warren, D. J. Keeble, *Solid-State Electron.*, **34**, 835 (1991).
80. E. H. Poindexter, *Semicond. Sci. Technol.*, **4**, 961 (1989).
81. M. Stutzmann, *Z. Phys. Chem. N.F.*, **151**, 211 (1989) (in English).
82. B. Henderson, *Defects in Crystalline Solids*, E. Arnold, London, U.K., 1972, Section 5.3.
83. G. D. Watkins, "EPR Studies of Lattice Defects in Semiconductors", in *Defects and Their Structure in Non-metallic Solids*, B. Henderson and A. E. Hughes, Eds., Plenum Press, New York, NY, U.S.A., 1976, p. 203.
84. G. D. Watkins, "EPR and Optical Absorption Studies in Irradiated Semiconductors", in *Radiation Damage in Semiconductors*, F. L. Vook, Ed., Plenum Press, New York, NY, U.S.A., 1968, pp. 67–81.
85. U. Kaufmann, J. Schneider, A. Räuber, *Appl. Phys. Lett.*, **29**, 312 (1976); U. Kaufmann, J. Schneider, *Festkörperprobleme*, **20**, 87 (1980).
86. H. C. Crookham, T. A. Kennedy, D. J. Treacy, *Phys. Rev.*, **B46**, 1377 (1992).
87. P. Turek, J.-J. André, A. Giraudeau, J. Simon, *Chem. Phys. Lett.*, **134**, 471 (1987).
88. X.-S. Tang, M. Moussavi, G. C. Dismukes, *J. Am. Chem. Soc.*, **113**, 5914 (1991).
89. A. M. Ziatdinov, *Mol. Phys. Rep.*, **18/19**, 149–157 (1997).
90. D. J. Newman, *Adv. Phys.*, **20**, 197 (1971).
91. D. J. Newman, W. Urban, *Adv. Phys.*, **24**, 793 (1975).
92. M. Moreno, *J. Phys. Chem. Solids*, **51**, 835 (1990).
93. Y. Y. Yeung, *J. Phys. C. Solid State Phys.*, **21**, 2453 (1988).
94. M. Heming, G. Lehmann, *Chem. Phys. Lett.*, **80**, 235 (1981); see also M. Heming, G. Lehmann, "Superposition Model for the Zero-Field Splittings of 3*d*-Ion EPR: Experimental Tests, Theoretical Calculations and Applications", in *Electronic Magnetic Resonance of the Solid State*, J. A. Weil, Ed., Canadian Society for Chemistry, Ottawa, ON, Canada, 1987, pp. 163–174.
95. J. M. Baker, A. A. Jenkins, R. C. C. Ward, *J. Phys. Condens. Matter*, **3**, 8467 (1991).
96. M. J. Mombourquette, J. A. Weil, *J. Chem. Phys.*, **87**, 3385 (1987).
97. J. Michoulier, J. M. Gaite, *J. Chem. Phys.*, **56**, 5205 (1972).
98. J. M. Gaite, "Study of the Structural Distortion around S-State Ions in Crystals, Using the Fourth-Order Spin-Hamiltonian Term of the EPR Spectral Analysis", in *Electronic Magnetic Resonance of the Solid State*, J. A. Weil, Ed., Canadian Society for Chemistry, Ottawa, ON, Canada, 1987, pp 151–174.
99. N. M. Nizamutdinov, N. M. Khasanson, G. R. Bulka, V. M. Vinokurov, I. S. Rez, V. M. Garmash, N. I. Ravlova, *Sov. Phys. Crystallogr.*, **32**, 408 (1987).
100. S. S. Eaton, K. M. More, B. M. Sawant, G. R. Eaton, *J. Am. Chem. Soc.*, **105**, 6560 (1983).
101. R. E. Coffman, A. Pezeshk, *J. Magn. Reson.*, **70**, 21 (1986).
102. Various authors, *Appl. Magn. Reson.*, **3**(2), 1–381 (1992).
103. R. W. Fessenden, R. H. Schuler, *J. Chem. Phys.*, **39**, 2147 (1963).
104. A. Hinchliffe, N. M. Atherton, *Mol. Phys.*, **13**, 89 (1967).
105. S. H. Glarum, J. H. Marshall, *J. Chem. Phys.*, **44**, 2884 (1966).

NOTES

1. There is confusion in the literature as to the usage of terms such as 'spin density' and 'spin population'. We prefer to use 'density' in the sense that dimensions of volume^{-1} are implied. Thus electron probability density has the units m^{-3}, and charge density has units $C\,m^{-3}$, and spin density has units m^{-3}. The term "spin population" is not recommended, since it can also suggest the Boltzmann distribution among the spin states. Rather, 'unpaired-electron population' is used herein to denote the unit-less quantity equaling the square of (unitless) wavefunction coefficients, or algebraic sums thereof (which can be negative).
2. We deal in this chapter with isotropic hyperfine splitting constants. For convenience, we drop the subscript 0 that indicates this.
3. Reference 2 applies and discusses the unrestricted self-consistent-field molecular-orbital scheme, based on the Hartree-Fock-Roothaan equations, which resorts to intermediate neglect of differential overlap (INDO).
4. However, various other effects enter. The Jahn-Teller distortion (Section 8.2), including vibronic coupling, and the nearby cation (e.g., K^+) affect the degeneracy.
5. See the series of papers by J. Kommandeur and co-workers, *J. Chem. Phys.*, **47**, 391–413 (1967).
6. Using relations such as Eq. 9.6 for adjacent as well as more distant carbon atoms.
7. In Chapter 4 we deal with the opposite extreme: the case in which the zero-field splittings arise entirely from spin-orbit coupling.
8. The silicon metal-oxide-semiconductor field-effect transistor (MOSFET) is a dominant device in the electronics industry. The whole unit can be mounted in a magnet, and the recombination of electrons and holes can be observed by monitoring its electrical characteristics: electrically detected magnetic resonance (EDMR) [79,80].
9. A higher value, $t_d = 16$, has more recently been recommended [93].
10. It is unusual to have two different hyperfine splittings for two hydrogen atoms bonded to the same carbon atom. This implies that Q is not the same for the two hydrogen atoms. An explanation for this effect has been proposed [104].

FURTHER READING

Relations Between Hyperfine Splittings and Spin Densities

N. M. Atherton, *Principles of Electron Spin Resonance*, Prentice-Hall, New York, NY, U.S.A., 1993. (Chapter 3 contains a quite detailed discussion of the relationship between spin density and unpaired-electron population.)

E. T. Kaiser, L. Kevan, Eds., *Radical Ions*, Wiley-Interscience, New York, NY, U.S.A., 1968. (Chapters 1, 4, 5 and 6 deal with spin densities, radical cations, orbital degeneracy in substituted benzenes, and anion radicals.)

J. D. Memory, *Quantum Theory of Magnetic Resonance Parameters*, McGraw-Hill, New York, NY, U.S.A., 1968, Chapters 7 and 8. Relations between hyperfine splittings and spin densities are treated in terms of valence-bond and molecular-orbital theories.

Organic Radicals

F. Gerson, W. Huber, *Electron Spin Resonance of Organic Radicals*, Wiley-VCH, Weinheim, Germany, 2003. (Chapter 3 covers spin densities and unpaired-electron populations.)

E. T. Kaiser, L. Kevan, Eds., *Radical Ions*, Wiley-Interscience, New York, NY, U.S.A., 1968.

Inorganic Radicals

P. W. Atkins, M. C. R. Symons, *The Structure of Inorganic Radicals*, Elsevier, Amsterdam, Netherlands, 1967.

J. R. Morton, "Electron Spin Resonance Spectra of Oriented Radicals", *Chem. Rev.*, **64**, 453 (1964).

PROBLEMS

9.1 The proton hyperfine splittings for the naphthalene anion are 0.495 and 0.187 mT (Section 3.2.2). Based on the molecular orbitals of naphthalene (Problem 9A.3), how should these hyperfine splittings be assigned? How does the ratio of hyperfine splittings compare with the ratio of the squares of the atomic-orbital coefficients for the molecular orbital containing the odd electron?

9.2 Given that the proton NMR transition energies in a free radical containing a proton with hyperfine splitting a_i are

$$h\nu = |g_p\beta_n B_i - g_e\beta_e a_i M_S| \tag{9.20}$$

where B_i is the NMR resonance field, derive Eq. 9.10 assuming that the energy-level populations are given by the Boltzmann distribution.

9.3 Proton NMR spectra of ethylbenzene at 56.4 MHz are shown in Fig. 9.13*a* without and in Fig. 9.13*b* with the corresponding monoanion as solute. From the shifts seen in the latter, confirm that the hyperfine splittings for the CH_2 and the *para* protons of the group are $+0.080$ and -0.087 mT, respectively. In this system, electron transfer is so rapid that all ethylbenzene molecules participate; the shifts are proportional to the mole fraction of the reduced form.

9.4 Calculate the unpaired-electron populations in the allyl radical, H_2CCHCH_2, from the Hückel molecular orbitals and energies given in Fig. 9A.1, taking $\lambda = 1.1$. Compare the results with the populations derived from the experimental hyperfine splittings [103] given below, taking $Q = -2.70$ mT. Assume that the smaller hyperfine splitting is positive, corresponding to a negative unpaired-electron population on the middle carbon atom. The two primary resonance structures of the allyl radical, with hyperfine

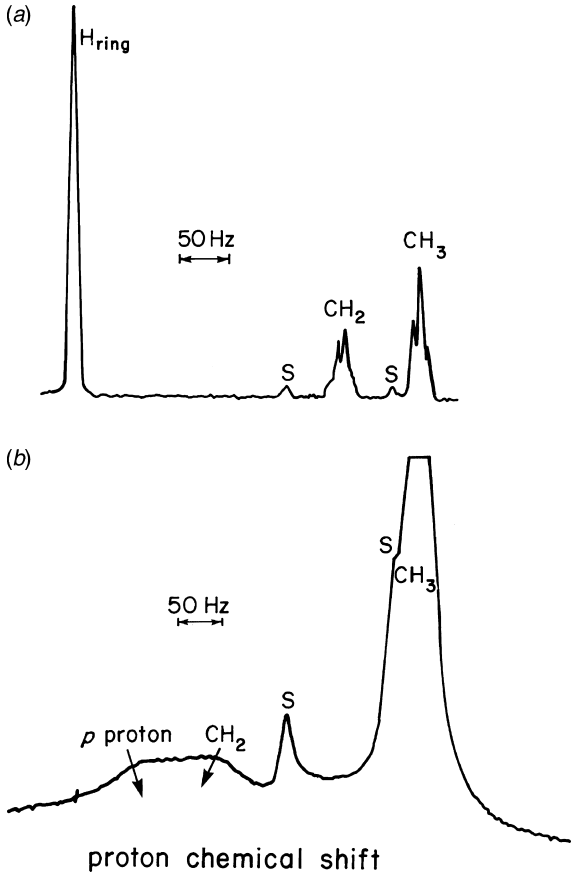

FIGURE 9.13 Proton magnetic resonance spectra at 56.4 MHz of (*a*) 1.93 M ethylbenzene, and (*b*) 1.93 M ethylbenzene plus 4.5×10^{-2} M ethylbenzene anion. The solvent is liquid d^8-tetrahydrofuran at $-75°C$. Peaks marked *S* are due to an impurity. [After E. de Boer, J. P. Colpa, *J. Phys. Chem.*, **71**, 21 (1967).]

splittings, are[10]

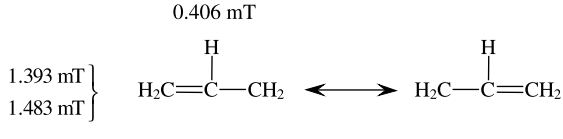

9.5 The proton hyperfine splittings for the 1,3-butadiene anion are -0.762 and -0.279 mT.

(***a***) What is the average value of Q?

(***b***) Explain why $|Q|$ is so low. (Usually Q ranges from -2.5 to -3.0 mT.)

9.6 The ^{1}H and ^{13}C hyperfine splittings (including the signs) have been measured [105] for the radical

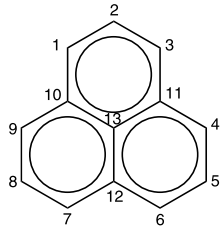

(**XI**) perinaphthenyl

$$a_1^{H} = -0.6270 \text{ mT} \quad a_2^{H} = 0.1833 \text{ mT} \quad a_1^{C} = 0.979 \text{ mT}$$
$$a_2^{C} = -0.792 \text{ mT} \quad a_{10}^{C} = -0.792 \text{ mT} \quad a_{13}^{C} = 0.332 \text{ mT}$$

The wavefunction for the non-bonded orbital is as follows:

$$\psi_{NB} = \frac{1}{\sqrt{6}}(\phi_1 - \phi_3 + \phi_4 - \phi_6 + \phi_7 - \phi_9)$$

(***a***) Assume $Q_{CH}^{H} = -2.7$ mT, and calculate ρ_1 and ρ_2.

(***b***) ρ_{10} and ρ_{13} have been computed from theory and are given as $\rho_{10} = -0.054$ and $\rho_{13} = +0.044$. Use this spin distribution to calculate the ^{13}C splitting constants. (Remember that positions 10 and 13 have three carbon atoms bonded to the central carbon, whereas positions 1 and 2 have two carbons and a proton.) How do these compare with the experimental ^{13}C splittings?

9.7 The statement has been made that the value of Q determines the total extent (Section 9.2.5) of the π-radical EPR spectrum. For the benzene anion the spectral extent is $\sim$2.25 mT, for CH_3 $\sim$6.9 mT, and for perinaphthenyl, $\sim$4.3 mT. Comment on the magnitudes of these values.

9.8 Interpret the spectrum shown in Fig. 9.8, which arises from the Cl_2^- ion in KCl.

APPENDIX 9A HÜCKEL MOLECULAR-ORBITAL CALCULATIONS

A brief summary of the HMO approach to the calculation of orbital energies and unpaired-electron distributions in π-electron systems is given here. Because of the crude assumption of non-interaction among the electrons, we can treat all anions, neutral molecules, and cations using the same theory. Thus the σ system of H_2^+,

H_2 and H_2^- can serve as one basic example; these calculations yield equations equally applicable to the π-electron states of the molecules $C_2H_4^+$, C_2H_4 and $C_2H_4^-$. This approach has been widely described in textbooks and in intermediate-level chemistry courses. Hence here we shall only map out successive steps and summarize intermediate and working-level expressions. Detailed molecular-orbital calculation procedures and tabulations of the results for many molecules are given in the references at the end of this appendix.

1. Define the molecular orbitals to be linear combinations

$$|\psi_i\rangle = c_{i1}|\phi_1\rangle + c_{i2}|\phi_2\rangle + \cdots + c_{in}|\phi_n\rangle \tag{9A.1}$$

of n normalized atomic orbitals. The total energy expectation value for the ith molecular orbital ($i = 1, \ldots, n$) is given by $\langle\psi_i|\hat{\mathcal{H}}|\psi_i\rangle$. We shall not need to establish the form of the hamiltonian $\hat{\mathcal{H}}$ explicitly. For the present we set $n = 2$; that is, we consider systems such as H_2 or the C_2H_4 π system for which one has two molecular orbitals

$$|\psi_1\rangle = c_{11}|\phi_1\rangle + c_{12}|\phi_2\rangle \tag{9A.2a}$$
$$|\psi_1\rangle = c_{21}|\phi_1\rangle + c_{22}|\phi_2\rangle \tag{9A.2b}$$

of interest. It is useful to define two parameters

$$H_{i,j} \equiv \langle\phi_i|\hat{\mathcal{H}}|\phi_j\rangle = H_{ji} \tag{9A.3a}$$
$$S_{i,j} \equiv \langle\phi_i|\phi_j\rangle = S_{ji} \tag{9A.3b}$$

in terms of the atomic orbitals ($i, j = 1, 2, \ldots, n$).

2. Determine the ratio of the coefficients c_i in each state (we suppress the first index here) by setting the derivatives $\partial U/\partial c_1$ and $\partial U/\partial c_2$ equal to zero. Then rewrite the two resulting equations in terms of the parameters H_{ij} and S_{ij} ($i, j = 1, 2$)

$$c_1(H_{11} - US_{11}) + c_2(H_{12} - US_{12}) = 0 \tag{9A.4a}$$
$$c_1(H_{12} - US_{12}) + c_2(H_{22} - US_{22}) = 0 \tag{9A.4b}$$

3. Set $H_{11} = H_{22}$, $S_{11} = S_{22} = 1$, and $S_{12} = 0$
4. Write determinantal equations

$$\begin{vmatrix} H_{11} - U & H_{12} \\ H_{12} & H_{11} - U \end{vmatrix} \tag{9A.5}$$

noting that c_1 and c_2 are the variables. Solution of the resulting determinant yields the energies

$$U_1 = H_{11} + H_{12} \tag{9A.6a}$$

$$U_2 = H_{11} - H_{12} \tag{9A.6b}$$

of the two levels. The ratio c_1/c_2 is found to be $+1$ for the orbital with energy U_1 and -1 for the orbital with energy U_2. The coefficient c_1 is determined by the normalization condition $\langle\psi|\psi\rangle = 1$. The final result is that the wavefunctions are

$$|\psi_1\rangle = \frac{1}{\sqrt{2}}(|\phi_1\rangle + |\phi_2\rangle) \quad \text{(energy } U_1\text{)} \tag{9A.7a}$$

$$|\psi_2\rangle = \frac{1}{\sqrt{2}}(|\phi_1\rangle - |\phi_2\rangle) \quad \text{(energy } U_2\text{)} \tag{9A.7b}$$

for the lower and the upper states, since H_{11} and H_{12} are both negative.

In the HMO description of ground-state H_2^+ and $C_2H_4^+$, the single electron occupies the lower level. For ethylene in its ground state, the two π electrons occupy the lower level of this diamagnetic molecule.

It is important to be able to establish the energy levels for linear conjugated systems of n atoms. Each of the n molecular orbitals is taken to be a linear combination of n atomic orbitals (Eq. 9A.1). The secular determinant is set equal to zero. The integrals H_{ij} and S_{ij} are the numerical parameters already encountered. Thus, generalizing Eq. 9A.5, one has

$$\begin{vmatrix} H_{1n} - US_{1n} & \cdots\cdots & \cdots\cdots & \cdots\cdots & H_{nn} - US_{nn} \\ \cdots\cdots & \cdots\cdots & \cdots\cdots & \cdots\cdots & \cdots\cdots \\ H_{13} - US_{13} & H_{23} - US_{23} & H_{33} - US_{33} & \cdots\cdots & H_{3n} - US_{3n} \\ H_{12} - US_{12} & H_{22} - US_{22} & H_{23} - US_{23} & \cdots\cdots & H_{2n} - US_{2n} \\ H_{11} - US_{11} & H_{12} - US_{12} & H_{13} - US_{13} & \cdots\cdots & H_{1n} - US_{1n} \end{vmatrix} = 0 \tag{9A.8}$$

where the rows are arranged in increasing order of the energy H_{ii}. The following simplifying assumptions are made:

1. $S_{ii} = 1$, $S_{ij} = 0$ if $i \neq j$.
2. All H_{ij} $(i \neq j) = \beta$ if atoms are bonded and zero otherwise. The numerical parameter β is called the *resonance integral* (a negative quantity).
3. All $H_{ii} = \alpha$. The numerical parameter α is called the *Coulomb integral* (a negative quantity).

These symbols, used as matrix elements, should not be confused with the spin functions α and β used elsewhere in this book.

Application of Eq. 9A.7 to the allyl molecule leads to the determinantal equation

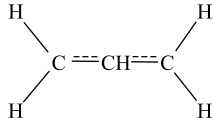

$$\begin{vmatrix} \alpha - U & \beta & 0 \\ \beta & \alpha - U & \beta \\ 0 & \beta & \alpha - U \end{vmatrix} = 0 \qquad (9A.9a)$$

On dividing all terms by β and making the substitution $x = (\alpha - U)/\beta$, one obtains the determinantal equation

$$\begin{vmatrix} x & 1 & 0 \\ 1 & x & 1 \\ 0 & 1 & x \end{vmatrix} = 0 \qquad (9A.9b)$$

The three eigenvalues, obtained by expansion of the determinant, and the corresponding wavefunctions are

$$U_3 = \alpha - \sqrt{2}\beta \quad \psi_3 = \frac{1}{2}\phi_1 - \frac{1}{\sqrt{2}}\phi_2 + \frac{1}{2}\phi_3 \qquad (9A.10a)$$

$$U_2 = \alpha \qquad \psi_2 = \frac{1}{\sqrt{2}}\phi_1 + 0\,\phi_2 - \frac{1}{\sqrt{2}}\phi_3 \qquad (9A.10b)$$

$$U_1 = \alpha + \sqrt{2}\beta \quad \psi_1 = \frac{1}{2}\phi_1 + \frac{1}{\sqrt{2}}\phi_2 + \frac{1}{2}\phi_3 \qquad (9A.10c)$$

The orbital energy levels for and spin configurations of the allyl radical, cation and anion are shown in Fig. 9A.1.

The coefficients for the set of corresponding molecular orbitals can be obtained from the secular determinant (Eq. 9A.9*b*) by writing each line as an equation and substituting each eigenvalue ($x = -\sqrt{2}$, 0 or $\sqrt{2}$) in turn, and by applying the normalization condition (Eq. 9.3)

Calculation of the four Hückle molecular orbitals and energies of 1,3-butadiene is given as a problem at the end of this appendix; the results are quoted in Table 9A.1.

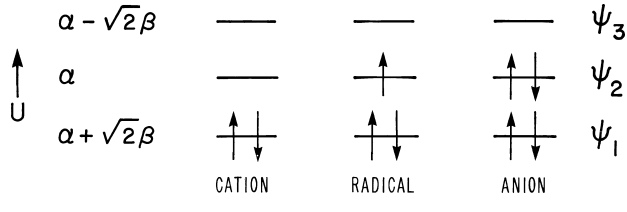

FIGURE 9A.1 The orbital energy levels of the allyl cation, radical and anion. Here ψ_i ($i = 1,2,3$) is the $2p_z$ atomic orbital on carbon atom i.

TABLE 9A.1 Molecular Orbitals and Energies of 1,3-Butadiene

Molecular Orbitals	Orbital Energies
$\psi_4 = 0.371\phi_1 - 0.600\phi_2 + 0.600\phi_3 - 0.371\phi_4$	$U_4 = \alpha - \frac{1}{2}(\sqrt{5}+1)\beta$
$\psi_3 = 0.600\phi_1 - 0.371\phi_2 - 0.371\phi_3 + 0.600\phi_4$	$U_3 = \alpha - \frac{1}{2}(\sqrt{5}-1)\beta$
$\psi_2 = 0.600\phi_1 + 0.371\phi_2 - 0.371\phi_3 - 0.600\phi_4$	$U_2 = \alpha + \frac{1}{2}(\sqrt{5}-1)\beta$
$\psi_1 = 0.371\phi_1 + 0.600\phi_2 + 0.600\phi_3 + 0.371\phi_4$	$U_1 = \alpha + \frac{1}{2}(\sqrt{5}+1)\beta$

TABLE 9A.2 Molecular Orbitals and Energies of Benzene

Molecular Orbitals	Orbital Energies
$\psi(b) = \frac{1}{\sqrt{6}}(\phi_1 - \phi_2 + \phi_3 - \phi_4 + \phi_5 - \phi_6)$	$U(b) = \alpha - 2\beta$
$\psi(e_2) = \frac{1}{2}(\phi_2 - \phi_3 + \phi_5 - \phi_6)$	$U(e_2) = \alpha - \beta$
$\psi(e_2) = \frac{1}{\sqrt{12}}(2\phi_1 - \phi_2 - \phi_3 + 2\phi_4 - \phi_5 - \phi_6)$	$U(e_2) = \alpha - \beta$
$\psi(e_1) = \frac{1}{2}(\phi_2 + \phi_3 - \phi_5 - \phi_6)$	$U(e_1) = \alpha + \beta$
$\psi(e_1) = \frac{1}{\sqrt{12}}(2\phi_1 + \phi_2 - \phi_3 - 2\phi_4 - \phi_5 + \phi_6)$	$U(e_1) = \alpha + \beta$
$\psi(a) = \frac{1}{\sqrt{6}}(\phi_1 + \phi_2 + \phi_3 + \phi_4 + \phi_5 + \phi_6)$	$U(b) = \alpha + 2\beta$

The neutral molecule has four π electrons. Following the rules, these must be assigned to the molecular orbitals of lowest energy (i.e., two to ψ_1 and two to ψ_2, since β is negative) to describe the ground state.

For other conjugated systems one may proceed in an analogous fashion. The secular determinant for linear conjugated systems contains the values $\alpha - U$ on the diagonal, with β one position off the diagonal, and zero elsewhere. For cyclic systems there are other non-zero off-diagonal terms. The resulting $n \times n$ determinant may easily be solved by computers; however, the task is simplified if the determinant is factorable; this can often be accomplished if of the symmetry properties of the molecule are employed using straightforward methods of group theory [A1,A2]. The π molecular orbitals of benzene (Table 9A.2) are entirely determined by symmetry. For further information regarding HMO theory, see Refs. A3–A8.

HMO References

A1. A. Streitwieser Jr., *Molecular Orbital Theory*, Wiley, New York, NY, U.S.A., 1961. [Chapters 2 and 3 describe in detail the procedures for calculations of orbital energies and wavefunctions of hydrocarbons. Chapter 4 describes refinements of the method and Chapter 5 deals with applications to molecules having hetero (N, O, S or halogen] atoms.

A2. F. A. Cotton, *Chemical Application of Group Theory*, 3rd ed., Wiley-Interscience, New York, NY, U.S.A., 1990. (The treatment of monocyclic systems in Chapter 7 is of special interest, as is Chapter 8, dealing with inorganic complexes).

A3. J. N. Murrell, S. F. A. Kettle, J. M. Tedder, *Valence Theory*, Wiley, New York, NY, U.S.A., 1965. (Chapter 15 deals with the π-electron theory of organic molecules. Section 15.8, "A Critique of Hückel Theory," gives some insight into the successes of the HMO approach.)

A4. L. Salem, *The Molecular Orbital Theory of Conjugated Systems*, Benjamin, New York, NY, U.S.A., 1966, Chapter 1.

A5. M. J. S. Dewar, *The Molecular Orbital Theory of Organic Chemistry*, McGraw-Hill, New York, NY, U.S.A., 1969, Chapter 5.

A6. C. A. Coulson, A. Streitwieser, *Dictionary of π-Electron Calculations*, Freeman, San Francisco, CA, U.S.A., 1965.

A7. E. Heilbronner, Jr. P. A. Straub, *Hückel Molecular Orbitals*, Springer, New York, NY, U.S.A., 1966.

A8. P. W. Atkins, *Molecular Quantum Mechanics*, 2nd ed., Oxford University Press, Oxford, U.K., 1983, Section 10.9.

HMO Problems

9A.1 Set up the secular equation for the cyclopropenyl (C_3H_3) radical and solve for the orbital energies. Draw an orbital energy diagram and show the distribution of electrons among the π orbitals.

9A.2 Set up the secular equation for the 1,3-butadiene and solve for the energies. Substitute the energies into the secular equations and determine the coefficients in the four π molecular orbitals (Table 9A.1).

9A.3 The seven lowest-lying Hückel molecular orbitals

$$\psi_n = c_{n1}\phi_1 + c_{n2}\phi_2 + c_{n3}\phi_3 + \cdots + c_{n10}\phi_{10}$$

are shown below for naphthalene, in order of increasing energy; a structure showing the atom numbering is given in Table 9.3.

ψ_n	c_{n1}	c_{n2}	c_{n3}	c_{n4}	c_{n5}	c_{n6}	c_{n7}	c_{n8}	c_{n9}	c_{n10}
ψ_7	0	−0.408	0.408	0	0	0.408	−0.408	0	0.408	−0.408
ψ_6	0.425	−0.263	−0.263	0.425	−0.425	0.263	0.263	−0.425	0	0
ψ_5	0.425	0.263	−0.263	−0.425	0.425	0.263	−0.263	−0.425	0	0
ψ_4	0	0.408	0.408	0	0	0.408	0.408	0	−0.408	−0.408
ψ_3	0.400	0.174	−0.174	−0.400	−0.400	−0.174	0.174	0.400	0.347	−0.347
ψ_2	0.263	0.425	0.425	0.263	−0.263	−0.425	−0.425	−0.263	0	0
ψ_1	0.301	0.231	0.231	0.301	0.301	0.231	0.231	0.301	0.461	0.461

(***a***) Without doing any calculations, sketch approximately the set of HMO energies for naphthalene, and show the orbital occupation by electrons for the −1, 0 and +1 charged species.

(***b***) Compare ψ_5 with ψ_6, and ψ_4 with ψ_7. What identities may be written for corresponding c_{ni} values of the related pairs of molecular orbitals?

(***c***) What is the significance of a zero value of c_{ni}?

(***d***) Sketch the locations of nodal planes for all these orbitals.

9A.4 Calculate the unpaired-electron populations at each of the carbon atoms in the benzyl radical ($C_6H_5CH_2$), taking into account the following attributes of odd-alternant hydrocarbons.

1. There are two possible numbers of starred atoms, depending on the starting point. Choose the configuration with the larger number of starred atoms.

2. The unpaired electron resides in a non-bonding orbital, for which one notes that (a) the molecular-orbital coefficients of unstarred atoms are zero, and (b) the sum of the molecular-orbital coefficients of atoms about a starred position is zero.

Starting at one of the starred atoms in the benzene ring, assign the relative values of coefficients at each atom. From the requirement that the sum of the squares of the coefficients is equal to 1, ascertain the unpaired-electron population at each position.